2019 Fall

"Advanced Physical Metallurgy"

- Non-equilibrium Solidification -

12.03.2019

Eun Soo Park

Office: 33-313
Telephone: 880-7221
Email: espark@snu.ac.kr
Office hours: by appointment

5.7.3 Phase separation

2-Amorphous phases

Polymer

(AFM)
PGMA/PS

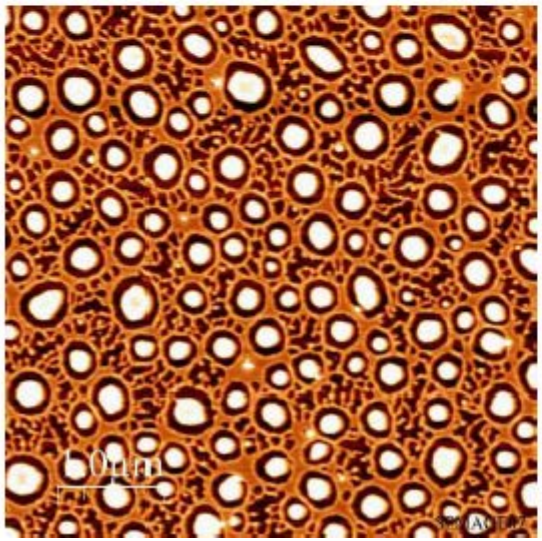

Oxide glass

(SEM)
SiO_2-NaO_2

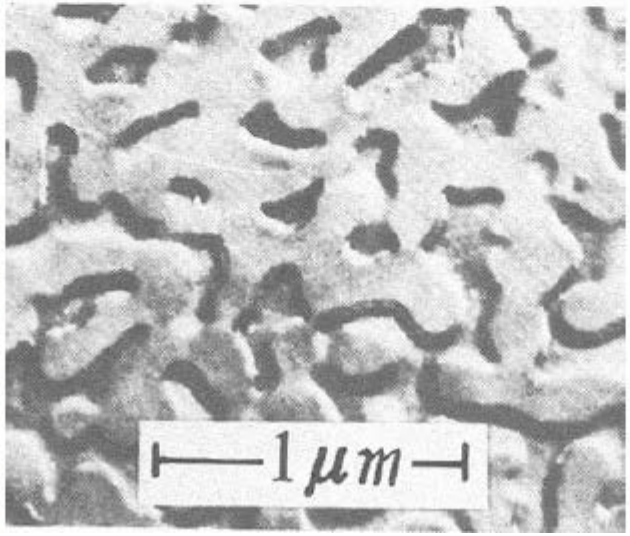

Metallic glass

(TEM)
TiYAlCo

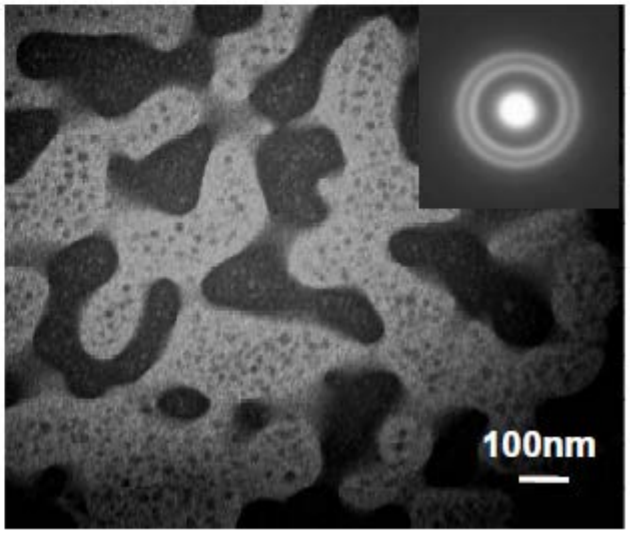

Annealing of Bulk Metallic Glasses: SR → SCLR (& PS) → Crystallization

5.7.3 Phase separation

* Miscibility gaps in phase separating system

- **Stable immiscibility**

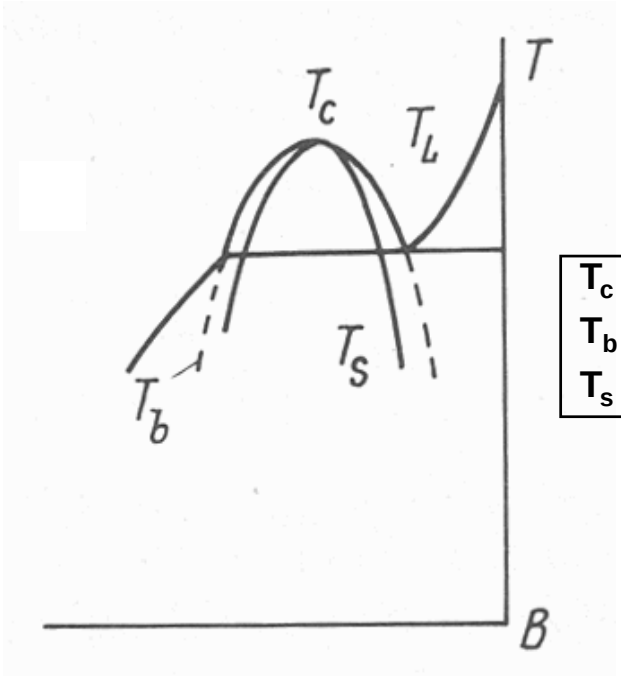

immiscibility above the liquidus

⇒ decomposition into stable liquid

T_c : critical temperature
T_b : binodal curve
T_s : spinodal curve

- **Metastable immiscibility**

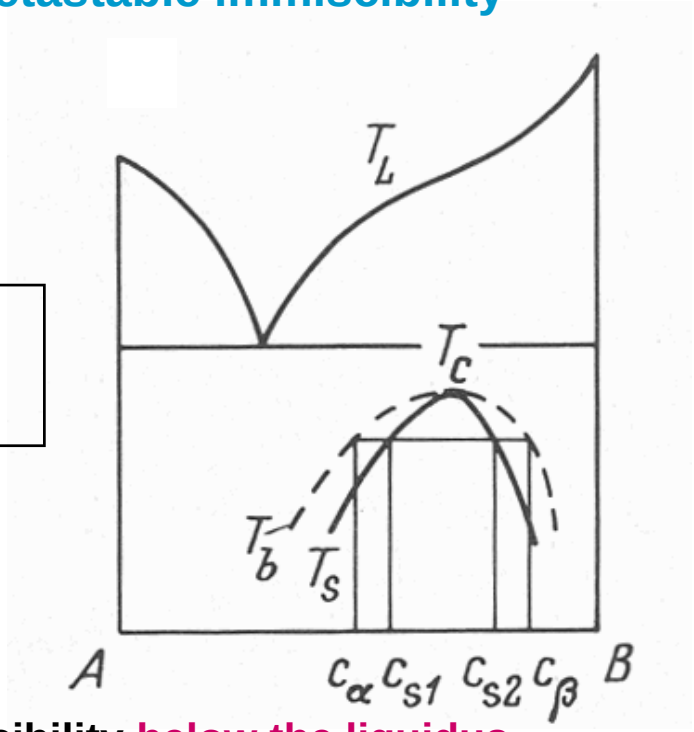

immiscibility below the liquidus

⇒ decomposition into metastable liquid

"Phase separation in glass" ed. by Mazurin and Porai-Koshits (1984)

(a) Positive heat of mixing relation among constituent elements

- **Alloy design considering heat of mixing relation among constituent elements**

$\Delta H_{mix} \gg 0$ between A & B

⬇

creates (meta)stable miscibility gap in limited composition range

⬇

Phase separation to A-rich & B-rich phase

- **Different two-phase structure by initial composition before phase separation**

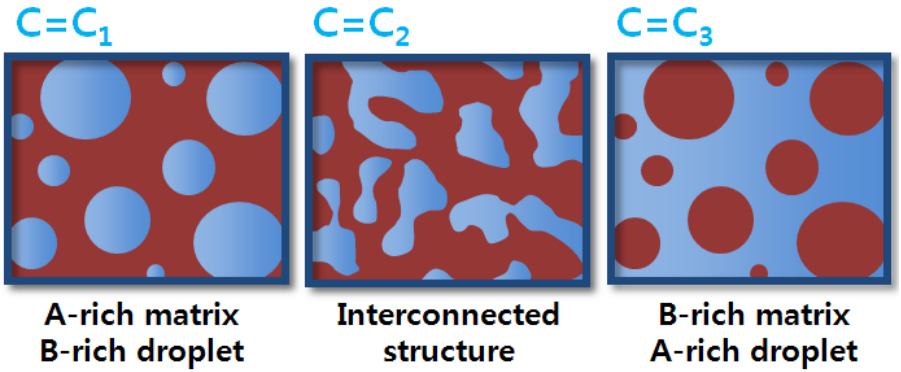

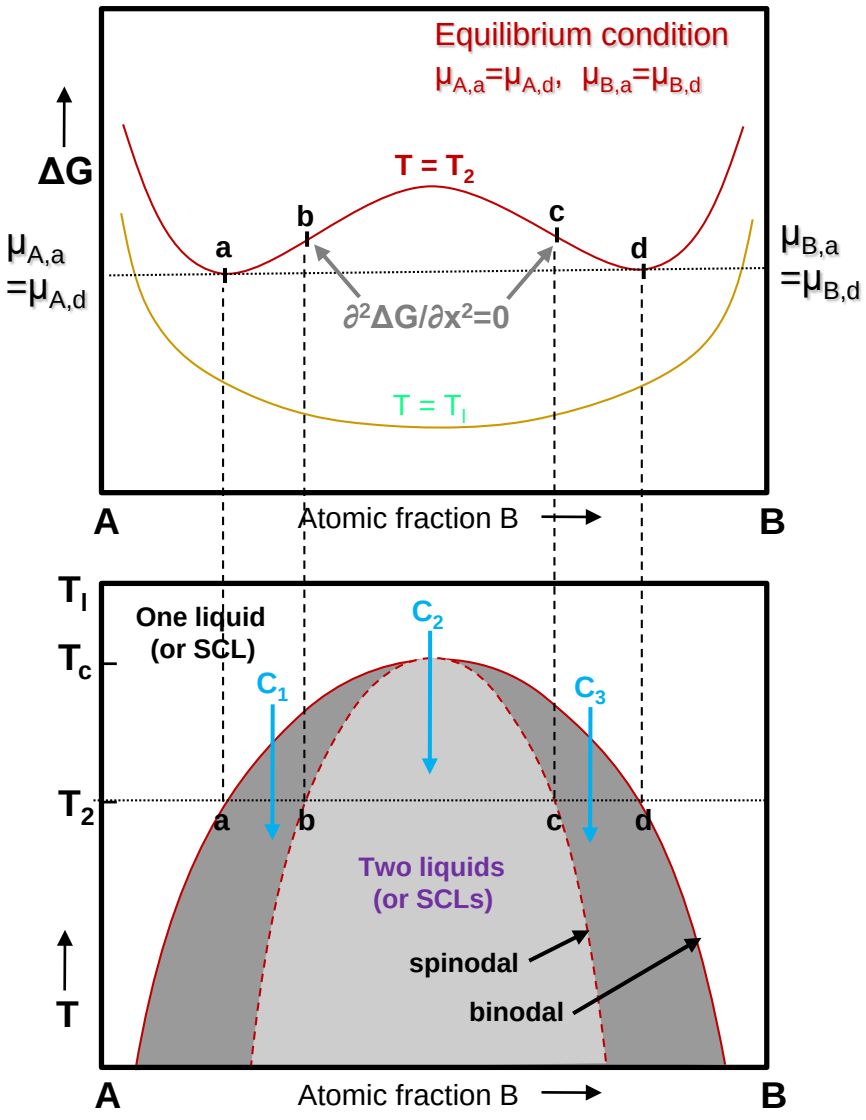

Nucleation and growth ↔ Spinodal decomposition without any barrier to the nucleation process

Microstructure determining parameters of phase separation in metallic glasses

- ❖Composition
- ❖Glass-forming ability of the separated liquid
- ❖Critical temperature
- ❖Asymmetry of the spinodal curve / Decomposition range

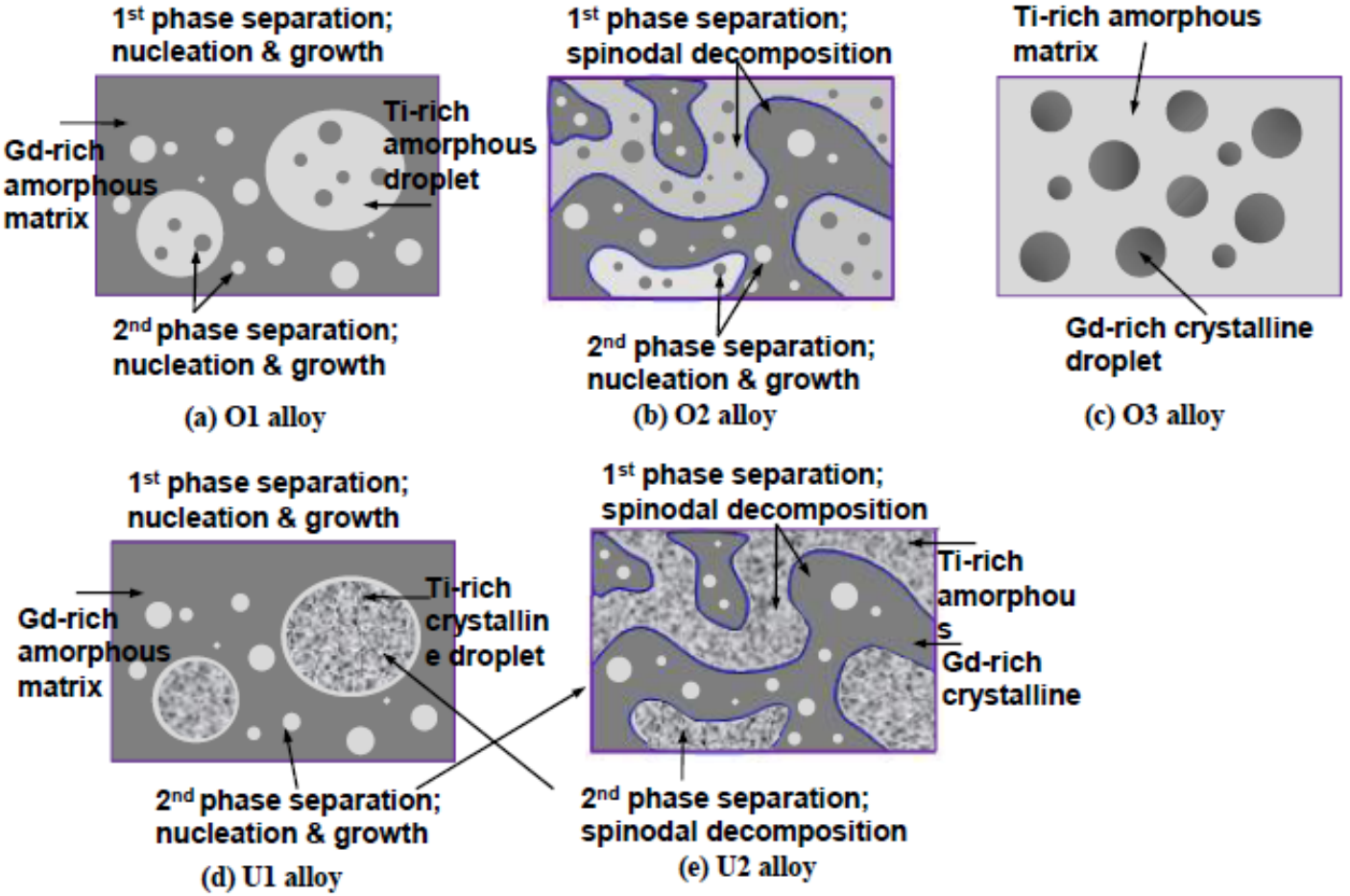

Effect of element with positive enthalpy of mixing among constituent elements

atomic scale heterogeneity

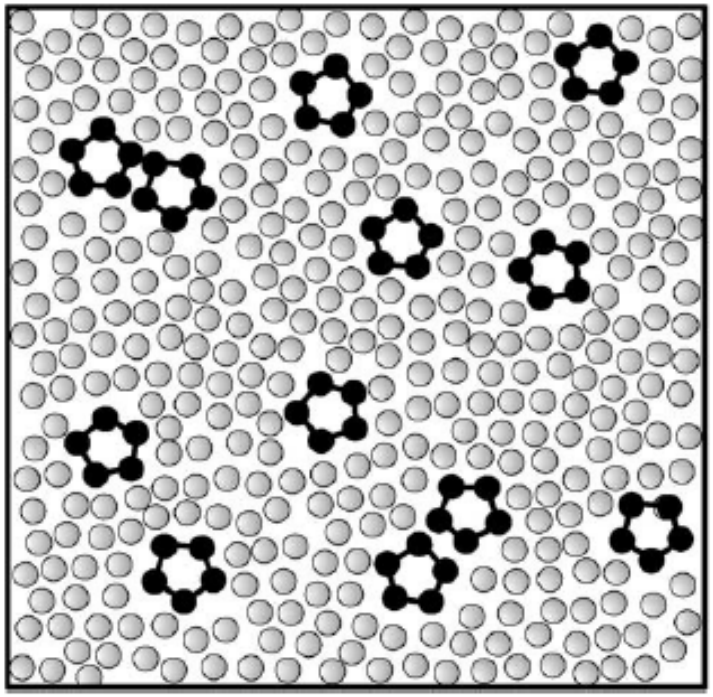

Enhancement of plasticity in BMGs

Phase separating metallic glasses

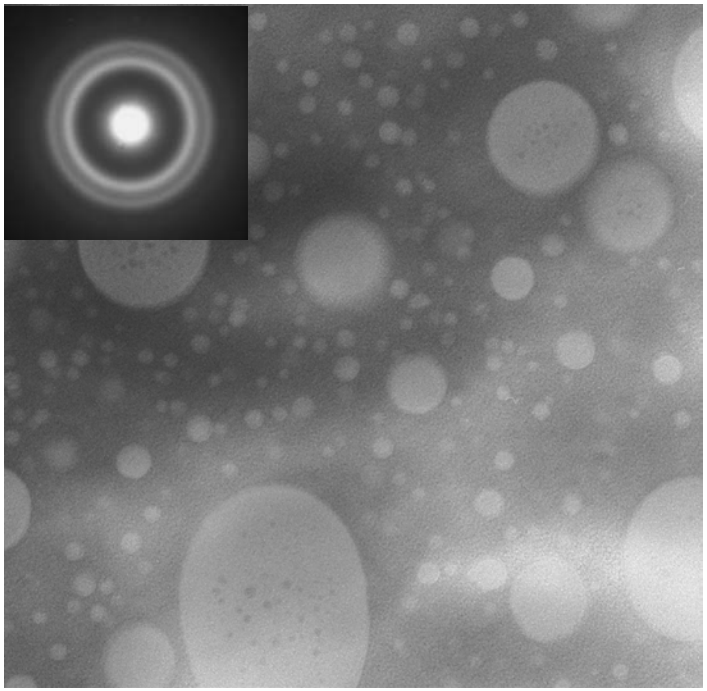

Unique properties

Movie of in-situ compression test using pico-indenter

- Particles prepared by dealloying $Gd_{27.5}Ti_{27.5}Al_{25}Co_{20}$ ribbon sample

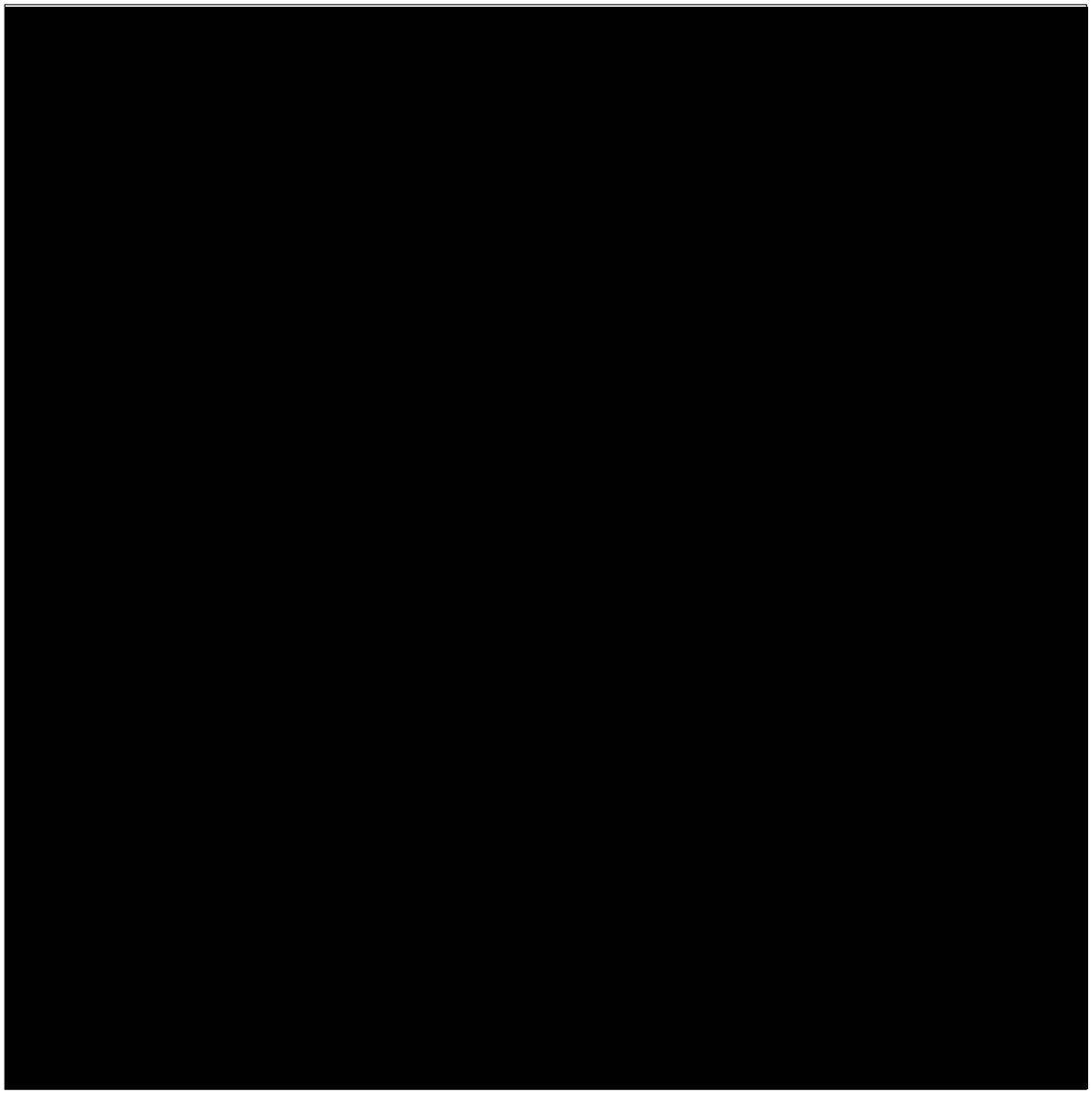

20x speed video from SEM imaging (15kV, Tilt angle : 2°)

5.7. Annealing of Bulk Metallic Glasses: SR → SCLR (& PS) → Crystallization

5.7.4 Crystallization: T_x ~ kinetic temperature, depends on the heating rate

- The nature of the crystalline phase produced on long time annealing was different depending on whether the annealing temperature was below Tg or above Tg.

→ In the glass state, the number of crystalline nuclei is constant, while in the supercooled liquid state, the nucleation rate is constant. In both the cases, the crystal nuclei grow through an interfacial reaction controlling process.

$$f = 1 - \exp\left(-kt^n\right)$$

k: 온도에 민감 $f(I, v)$ $\quad -\frac{\pi}{3} I v^3$

n: 1 ~ 4 (depend on nucleation mecnanism)

Growth controlled. | Nucleation-controlled.

n value is not constant, but is increasing continuously from 3.0 to 3.7 with increasing T_a.

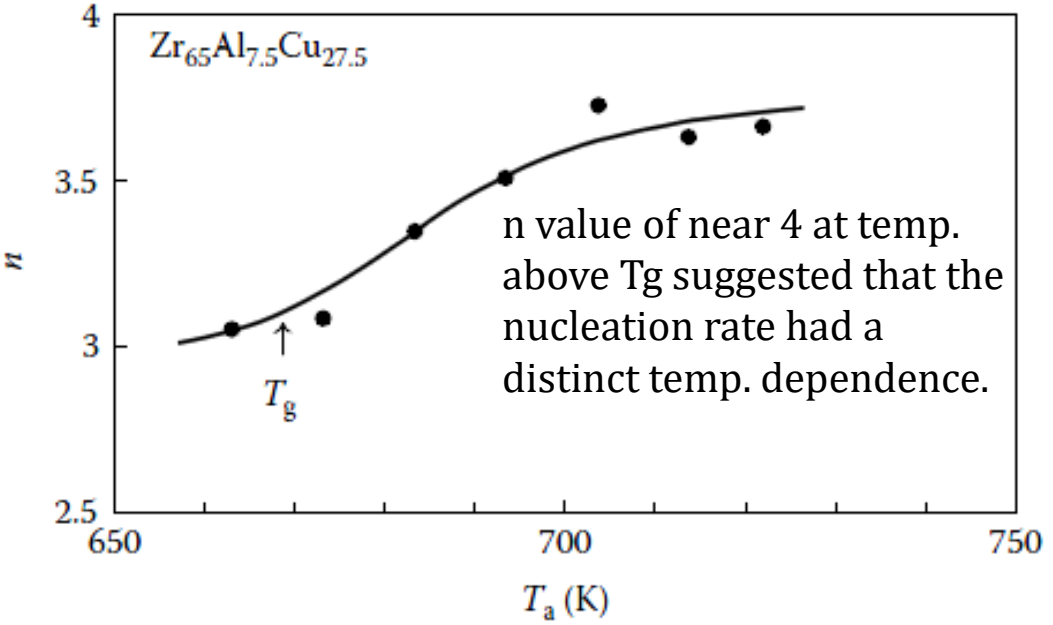

FIGURE 5.21
Variation of the Avrami exponent, n with annealing temperature, T_a during the isothermal annealing of glassy $Zr_{65}Al_{7.5}Cu_{27.5}$ alloy.

The nucleation rate is a function of both t_a and T_a. For isothermal annealing, the nucleation rate, $I(t_a)$ as a function of annealing time, t_a, at any temperature can be expressed according to the equation

$$I(t_a) = I_0 \exp\left(-\frac{\tau}{t_a}\right) \tag{5.9}$$

where

I_0 is the steady-state homogeneous nucleation rate

τ is the incubation time

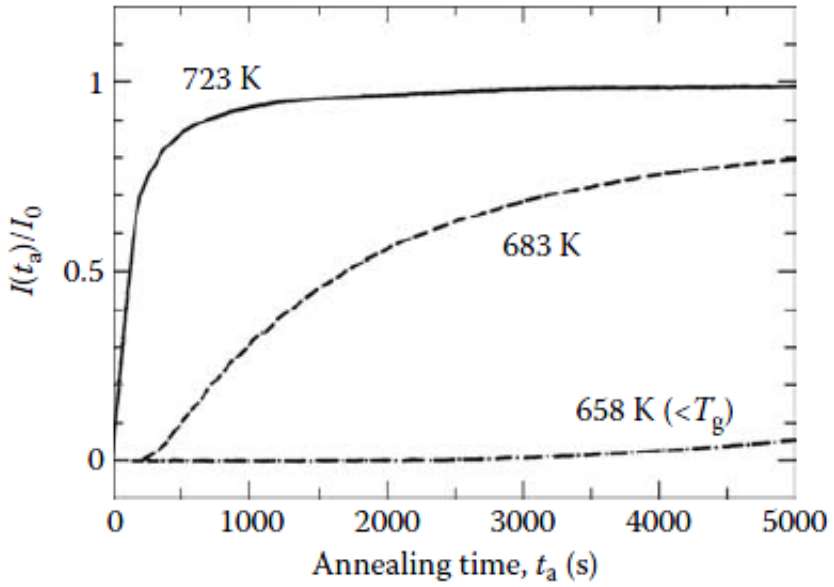

FIGURE 5.22
Variation of the reduced homogeneous nucleation rate, $I(t_a)/I_0$ evaluated from the incubation time for the precipitation of the $Zr_2(Cu,Al)$ phase with annealing time, t_a for the glassy $Zr_{65}Al_{7.5}Cu_{27.5}$ alloy annealed at 658, 683, and 723 K.

* **Non-Arrehenius-type thermal activation process**: The activation energy was calculated to change from 400 kJ/mol in the glassy solid to 260 kJ/mol in the supercooled liquid state for the nucleation of the Zr_2Cu and ZrAl phases, and from 370 kJ/mol in the glassy solid to 230 kJ/mol in the supercooled liquid state for crystallization.

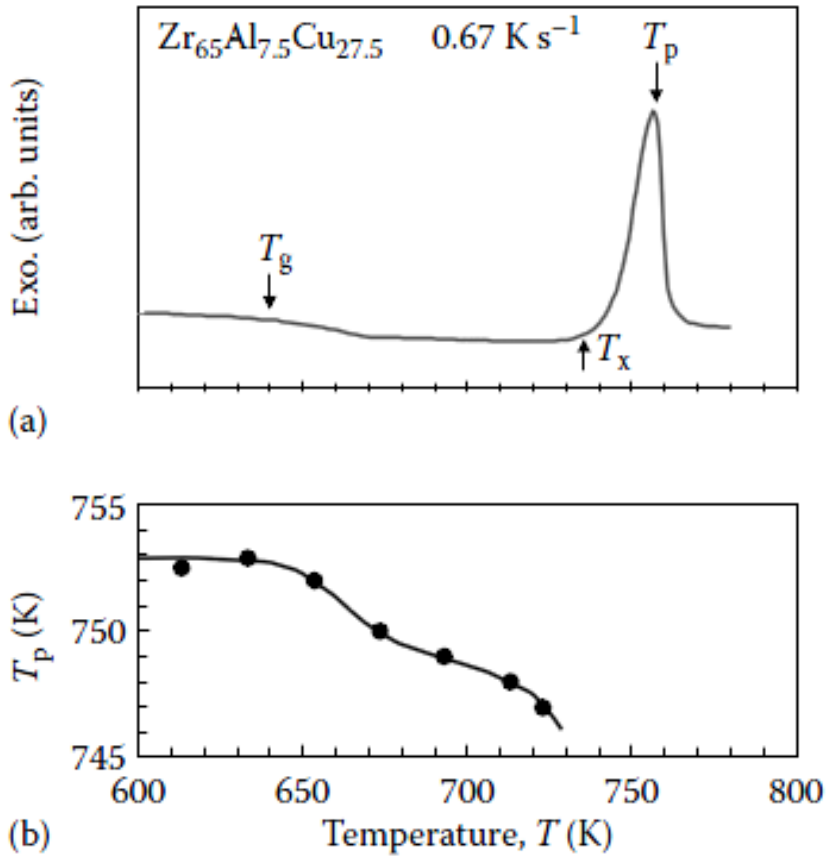

FIGURE 5.23
(a) DSC plot of the $Zr_{65}Al_{7.5}Cu_{27.5}$ glassy alloy continuously heated at a rate of 0.67 K s^{-1} (40 K min^{-1}). The T_g, T_x, and T_p values are indicated. (b) Variation of the peak temperature, T_p in the exothermic reaction due to crystallization with heating temperature, T_a.

* **The peak temperatures for nucleation and growth are well separated for glassy alloys exhibiting a significant width of the supercooled liquid region (ΔTx)**, where as for glassy alloys that do not show a Tg, these two peak temperatures overlap. This difference is expected **to reflect in the nature of the crystallized product** obtained from the supercooled liquid region. Accordingly, **the crystallized structure was examined as a function of the heating rate.**

---

* In $Zr_{65}Al_{7.5}Cu_{27.5}$ with large ΔT_x, the contribution to the growth rate increases with increasing heating rate as compared with the contribution to the nucleation rate. However, no significant change in the grain size of the Zr_2Cu phase with heating rate is seen for the $Zr_{67}Cu_{33}$ alloy with the much smaller ΔTx.

→ **Thus, the increase in the contribution to the growth rate with increasing heating rate becomes significant at temperatures just below Tx in the wide supercooled liquid region.**

- **Annealed for 1020s (17min) at 693K (above Tg): BCT Zr_2Cu phase precipitated in SCLR**/ dendritic morphology with a preferential growth direction, indicating that the redistribution of the constituent elements at the liquid-solid interface was necessary for the growth of the crystalline phase.
- **Annealed for 780 ks (9 days) at 613 K (below Tg): Zr_2Cu phase precipitated in the glassy solid**/ a nearly spherical morphology with rather smooth interface, suggesting that the growth of the Zr2Cu phase took place in the absence of significant redistribution of the constituent elements at the interface between Zr2Cu and the glassy phases/ more homogeneous distribution of Zr2Cu

---

* **The structure and morphology of the crystallized phases also appear to be a function of the Al content in the alloy.**

5.8 Effect of Environment: especially in the case of reactive glasses, for example, those based on Zr and Fe.

- In $Fe_{77}Gd_3B_{20}$ ribbon, the significant difference in the crystallization behavior was attributed to **surface oxidation, which reduces their thermal stability.**

- In $Zr_{41}Ti_{14}Cu_{12.5}Ni_{10}Be_{22.5}$, the crystallization of the glassy phase started earlier with decreasing air pressure during annealing due to deeper oxygen penetration at low pressure./ Oxygen is know to speed up the crystallization process by promoting extra heterogeneous sites for nucleation. When the oxygen pressure was low , the thickness of the surface oxide layer was small and therefore more oxygen could diffuse inside and accelerate the crystallization process.
  → The crystallization kinetics were faster at low partial pressure of oxygen.

- **The presence of oxygen in the alloys has a significant effect on the nature of the phases formed after quenching and also those formed on crystallization.** Therefore, it is essential that the alloys are clean and devoid of impurities, especially in active metals. Otherwise comparison between results by different investigators becomes difficult.

5.9 Effect of Pressure during Annealing

- hot pressing, hot extrusion, hot isostatic pressing, and other recently developed methods such as spark plasma sintering
- becomes useful to evaluate the thermal stability of glasses when exposed to high pressures
- critical for optimizing the consolidation process parameter or deforming in the supercooled liquid region

* Four different effects of pressure during annealing

1. Since there is an increase in the density of the product on crystallization (the glassy alloys are about 1%–2% less dense than their crystalline counterparts), it is natural to expect that the application of pressure would reduce the free volume in the glassy phase and therefore it is expected that crystallization will be accelerated. Such a process could easily happen when the glass crystallizes by a polymorphous mode.
2. Due to the retarded mobility of atoms (diffusivity) under high pressures, atomic diffusion is reduced and therefore crystallization is retarded as evidenced by the increase of crystallization temperatures. Since atomic diffusion is required for primary and eutectic-type crystallization modes, the application of pressure is expected to retard the crystallization of metallic glasses when the transformation takes place by any of these modes.

3. The relative Gibbs free energies of the glassy and other competing crystalline phases and also the activation barriers could be altered by the application of pressure. Consequently, metastable phases could form, the relative amounts of the different phases could be different, or alternately, different crystallization paths could be followed. The situation will be decided by the sign and magnitude of the variation of the crystallization temperature with pressure, that is, dT_x/dP.

   As an example, during the primary crystallization of Fe–B glassy alloys, α-Fe is formed at atmospheric pressure. However, when crystallization is conducted at pressures above 100 kbar, the formation of the metastable hcp ε-Fe phase was found to form [148]. Similarly, instead of the equilibrium tetragonal Nb_3Si phase, the cubic A15 Nb_3Si phase formed in the Nb–Si system during crystallization at high pressures in the glassy Nb–Si alloys [149]. Again, in the case of the crystallization of the $Zr_{41}Ti_{14}Cu_{12.5}Ni_{10}Be_{22.5}$ glassy alloy, Yang et al. [150] reported that the primary crystallized phase was the same at all pressures studied, but the subsequent phase-formation sequence was different at different temperatures.

4. The last effect of the application of pressure to metallic alloys is that amorphization could occur, that is, pressure-induced amorphization takes place [151–153]. For example, Wang et al. [151] reported that by cooling the $Zr_{41}Ti_{14}Cu_{12.5}Ni_{10}Be_{22.5}$ liquid at a high pressure of 6 GPa, they were able to obtain a high-density glassy alloy that had a structure and properties different from the low-density glassy alloy obtained by water quenching the melt.

TABLE 5.6

Effect of Pressure in Increasing the Crystallization Temperature of Bulk Metallic Glasses

Composition	Pressure Range Used (GPa)	Rate of Increase of T_x(K GPa^{-1})	Reference
$Al_{89}La_6Ni_5$	0–4	Decrease at a rate of 50 between 0 and 1 GPa and then increase at a rate of 25	[154]
$Fe_{72}P_{11}C_6Al_5B_4Ga_2$	0–2.4	30 (T_x dropped at higher pressures between 2.4 and 3.2)	[147]
$Mg_{60}Cu_{30}Y_{10}$	0–4	16	[155]
$Pd_{40}Ni_{40}P_{20}$	0–4.2	11	[156]
$Pd_{40}Cu_{30}Ni_{10}P_{20}$	0–4	11	[157]
$Zr_{66.7}Pd_{33.3}$	0–4	22	[135]
$Zr_{70}Pd_{30}$	0–3	11 ± 3 for quasicrystalline phase 9 ± 4 for intermetallic phase	[158]
$Zr_{65}Al_{7.5}Ni_{10}Cu_{7.5}Ag_{10}$	0–4.2	9.4 for T_{x1} No change for T_{x2}	[159]
$Zr_{48}Nb_8Cu_{14}Ni_{12}Be_{18}$	0–4.4	9.5	[160]
$Zr_{41.2}Ti_{13.8}Cu_{12.5}Ni_{10}Be_{22.5}$	0–3	19	[161]
$Zr_{46.8}Ti_{8.2}Cu_{7.5}Ni_{10}Be_{27.5}$	0–4.2	1.7	[162]
$Zr_{41}Ti_{14}Cu_{12.5}Ni_{10}Be_{22.5}$	0.5–6.5	12.8 (a sudden drop occurred at 5.6 GPa)	[150]

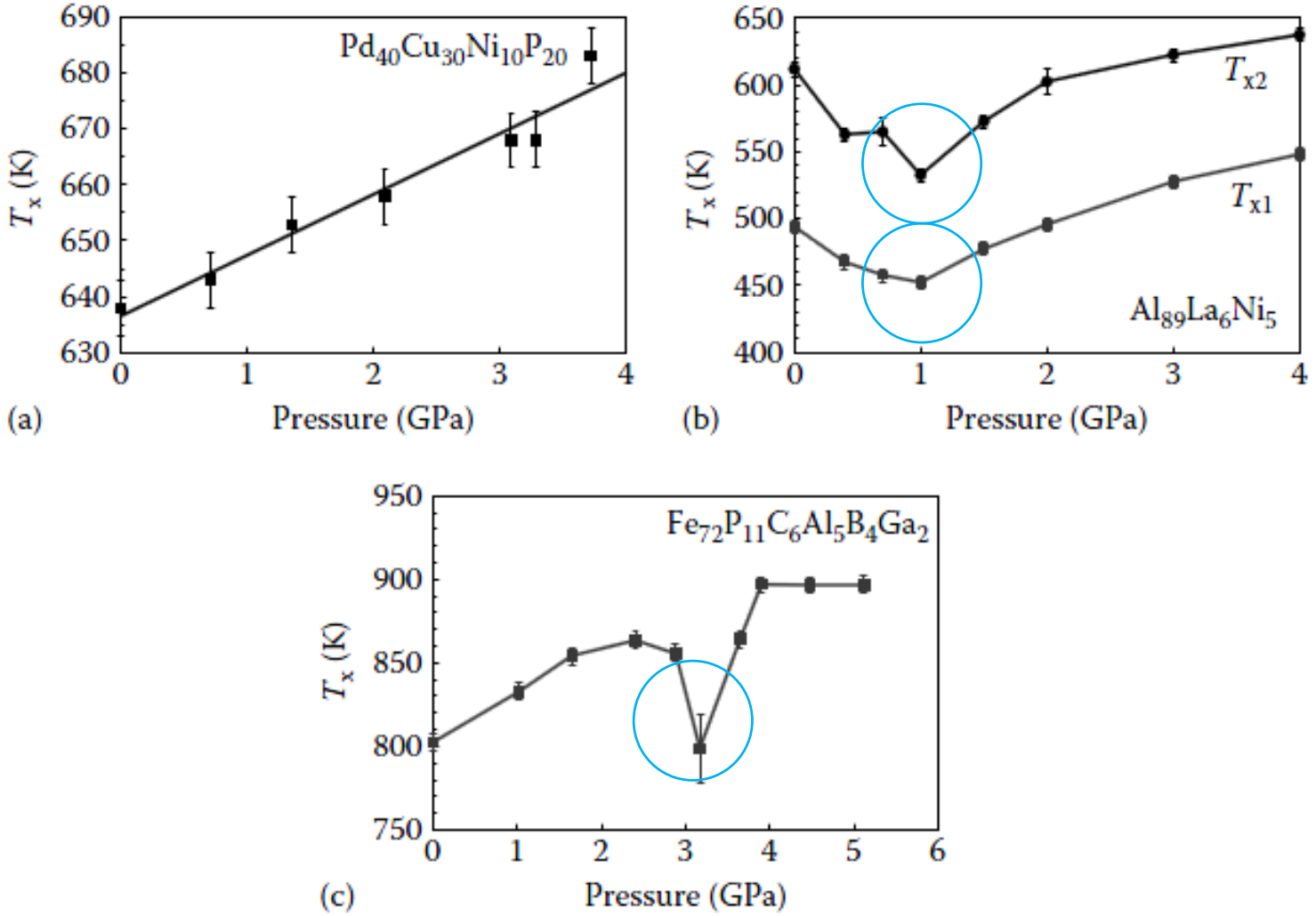

FIGURE 5.24

Variation of T_x with pressure in bulk metallic glassy alloys. Note that the T_x usually increases with increasing pressure although there are cases where either a decrease or no change has also been observed. Three typical examples are shown in (a) $Pd_{40}Cu_{30}Ni_{10}P_{20}$ glass, (b) $Al_{89}La_6Ni_5$ glass, and (c) $Fe_{72}P_{11}C_6Al_5B_4Ga_2$ glass. (Reprinted from Jiang, J.Z. et al., *J. Appl. Phys.*, 87, 2664, 2000. With permission.)

The rate of nucleation, I can be represented by the equation

$$I = I_0 \exp\left(-\frac{\Delta G^* + \Delta G^d}{RT}\right)$$

where

I_0 is a constant

ΔG^* is the thermodynamic activation barrier, that is, free energy required to form the critical nucleus

ΔG^d is the activation energy for diffusion (to transport atoms across the interface)

R is the universal gas constant

T is the temperature

$\Delta G^* + \Delta G^d = \Delta G$ is the total energy required for the nucleation

$$\Delta G^* = \frac{16\pi\sigma^3}{3\Delta G_v^2} = \frac{16\pi\sigma^3}{3(G_c - G_a)^2}$$

where

σ is the interfacial energy between the amorphous and crystalline phases

G_c and G_a are the Gibbs free energies of the crystalline and amorphous phases, respectively

At a given temperature and pressure, ΔG^* can be expressed as

$$(\Delta G^*)_{P,T} = \frac{16\pi\sigma^3 (V_c)^2}{3\left[P(V_a - V_c) - \Delta G^{a\to c} + E\right]^2}$$

where

V_c and V_a are the molar volumes of the crystalline and amorphous phases, respectively $\Delta G^{a\to c} = G_c - G_a$

E is the elastic energy induced by the volume change when the phase transformed from the amorphous to the crystalline state

Assuming a negligible pressure dependence of $\Delta G^{a\to c}$, E, and σ, we can see that ΔG^* decreases with increasing pressure and therefore crystallization is favored.

$$\left(\frac{\partial G}{\partial P}\right)_T = -\frac{32\pi\sigma^3}{3(\Delta G^{a\to c})^3}(V_c - V_a) + \left(\frac{\partial \Delta G^d}{\partial P}\right)_T$$

$V_c < V_a$

$-$ $-$ $+$ $+$

Whether increasing pressure promotes or retards crystallization is determined by the magnitudes of the two terms.

Ex) polymorphous mode→no atomic redistribution → always promotes crystallization

Homework:

Summary (page 265 – page 360)

Chapter 6_Physical Properties & Chapter 7_Corrosion Behavior

density, thermal expansion,

diffusion, electrical resistivity

specific heat, viscosity

You should submit your summary until 24 December. ☺

Deformation behavior: crystalline VS. amorphous

Crystalline

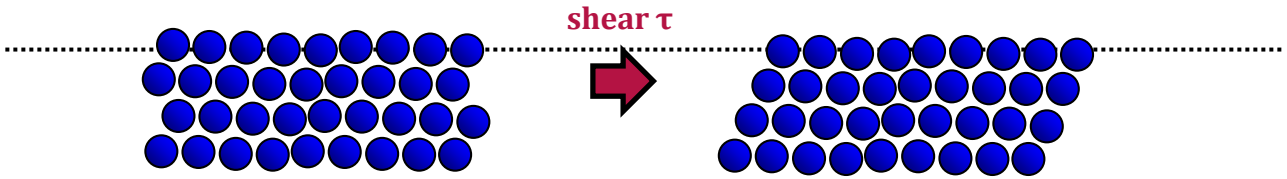

ordered structure — constant volume

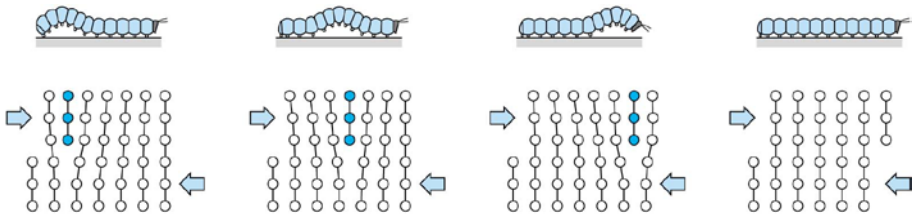

Dislocation motion in crystalline metal

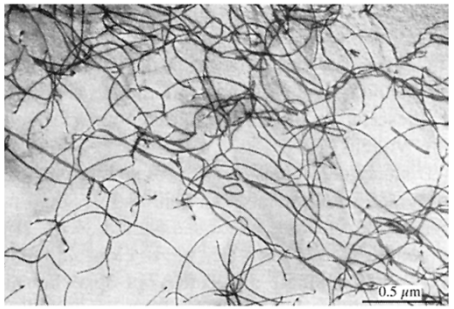

Dislocations

- "Incrementally breaking bonds"
- Has relatively low strength, performs work hardening
- Slip plane + Slip direction = Slip system
  (preferred crystallographic planes and directions)

Amorphous metal do not have slip system.

How to deform ?

Amorphous

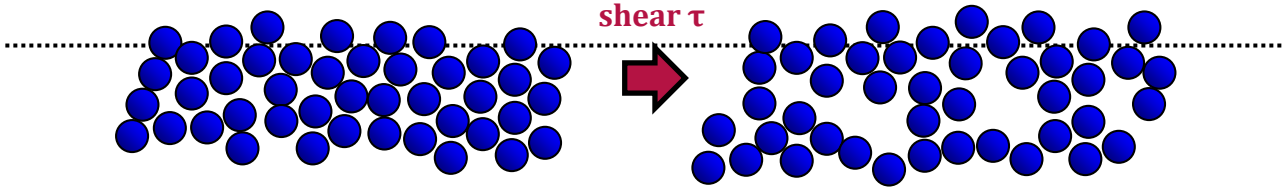

random structure — increase free volume (dilatation)

a) High strength of Bulk Metallic Glasses

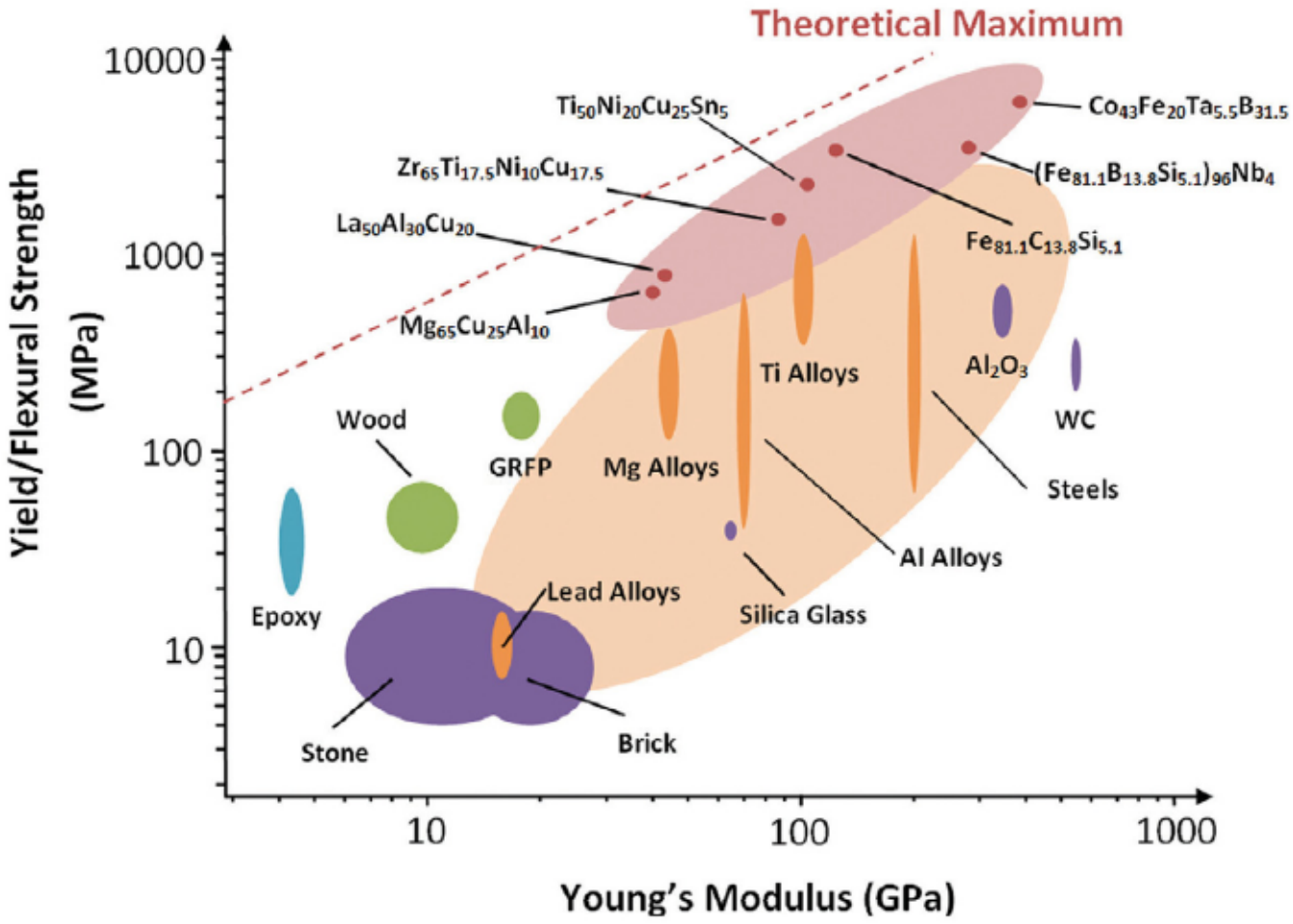

High fracture strength over 5 GPa in Fe-based BMGs

A.L. Greer, E. Ma, MRS Bulletin, 2007; 32: 612.

2) Large elastic strain limit of BMGs

Elastic Strain Limit

[as % of Original Shape]

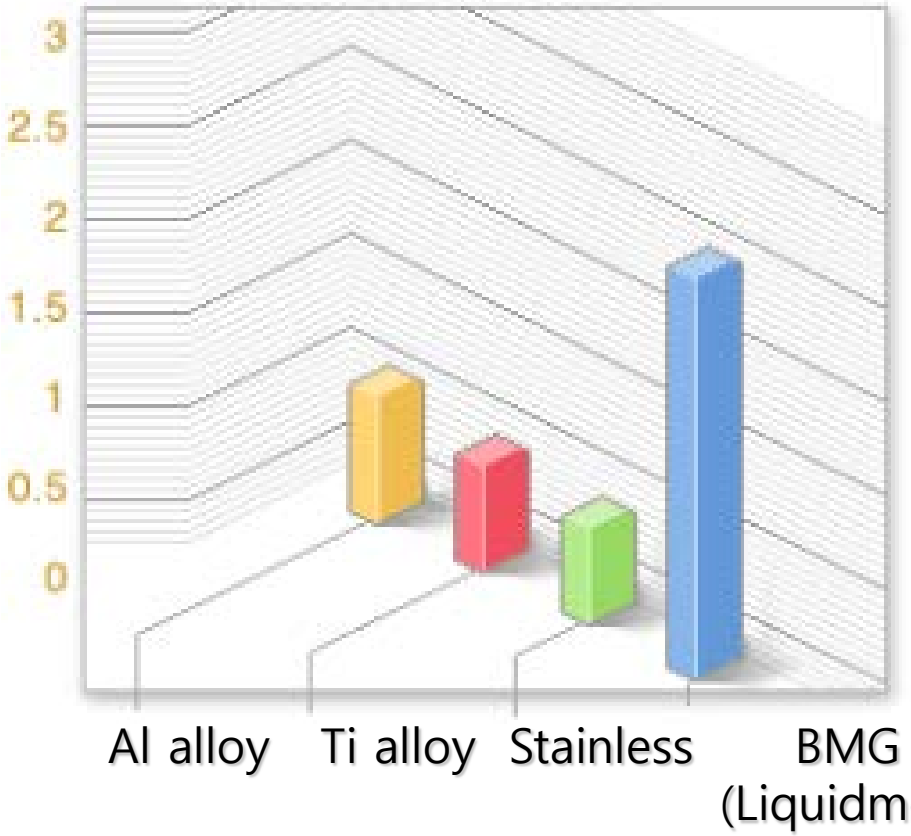

Stress-Strain Curve

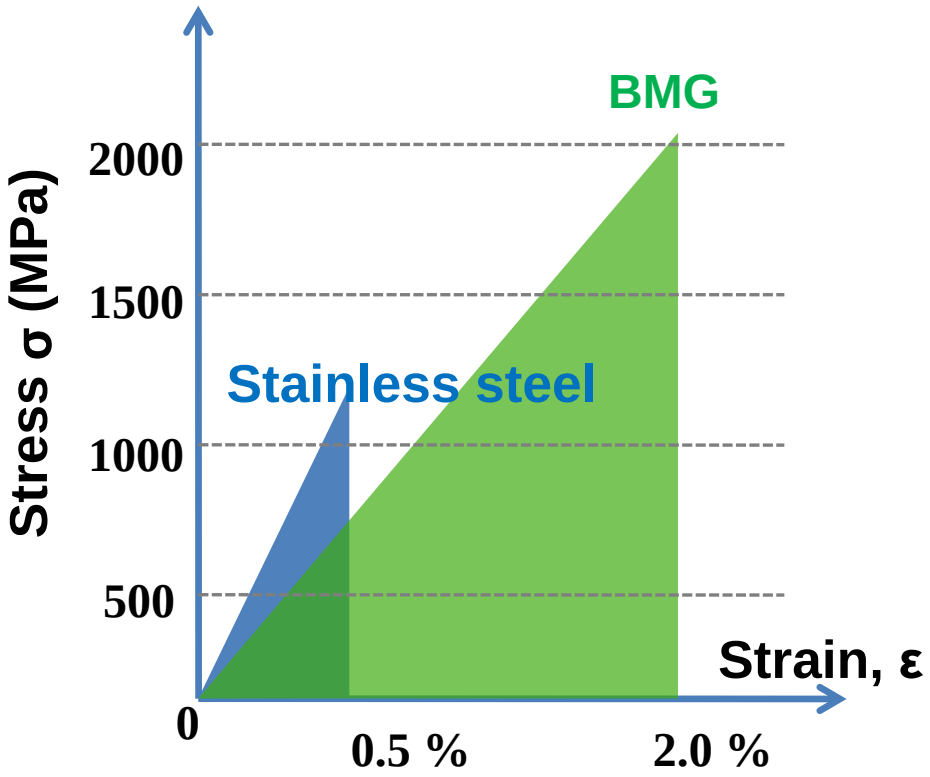

* BMGs with high strength & high elastic limit

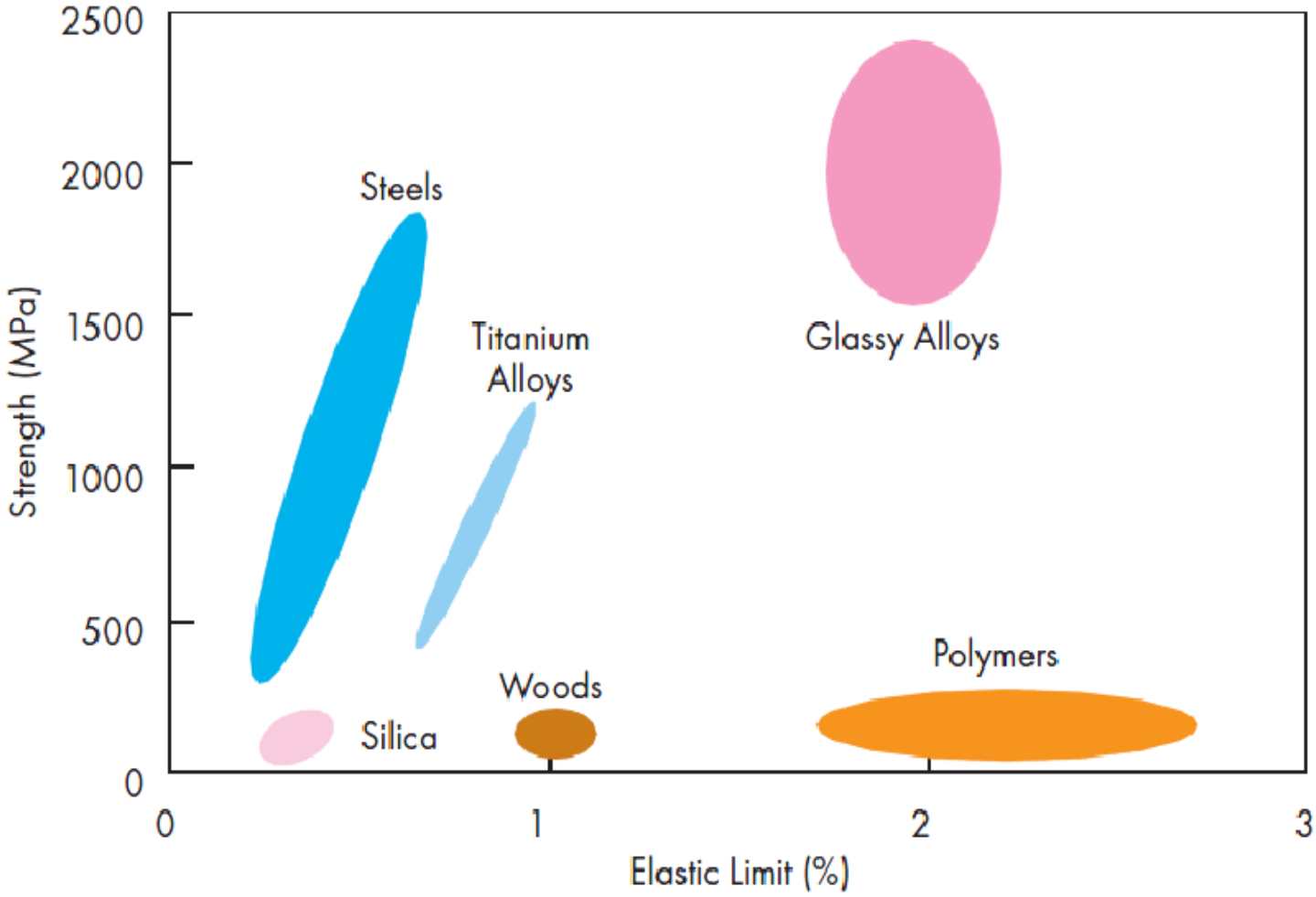

: Metallic Glasses Offer a Unique Combination of High Strength and High Elastic Limit

Drawback of BMGs as a Structural Materials

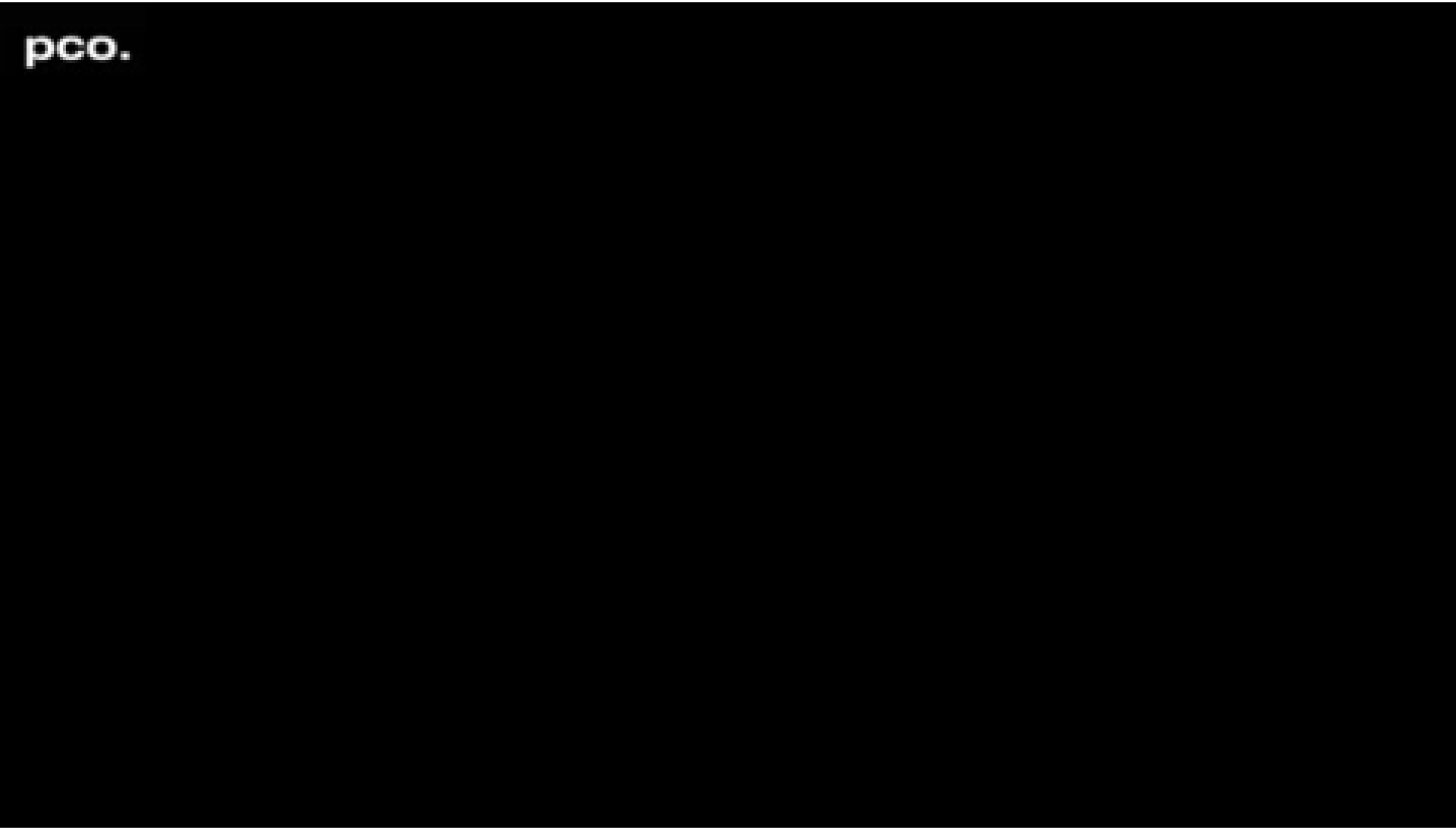

Limited plasticity by shear softening and shear band

- Microscopically brittle fracture

  ➡ Death of a material for structural applications

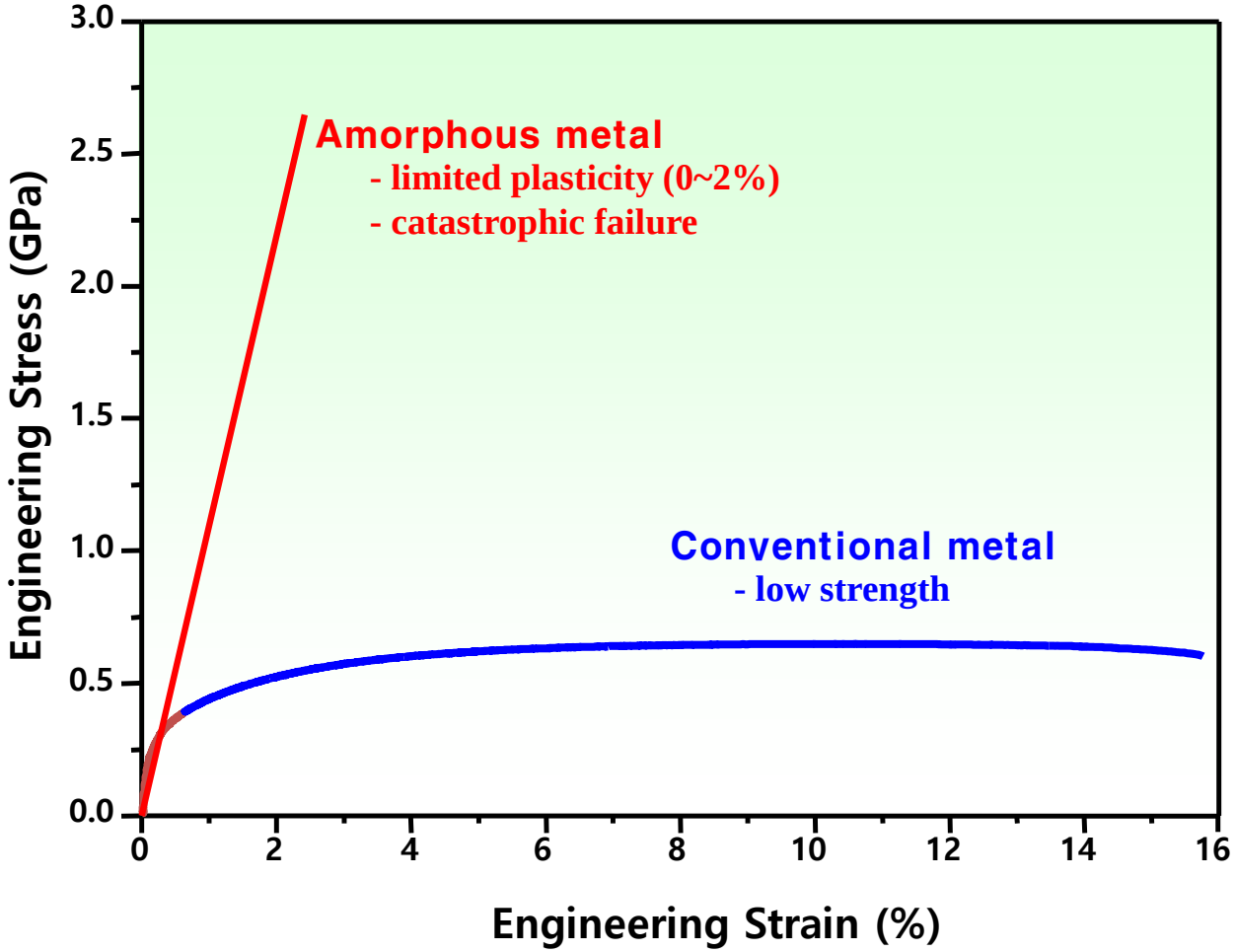

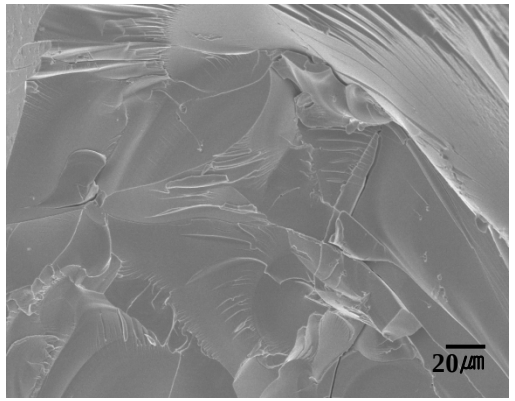

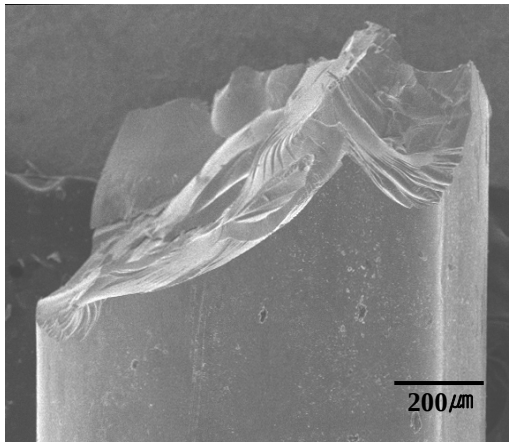

8.2 Deformation Behavior

Deformation behavior of Metallic glass

8.2.2 Homogeneous Deformation

- high temp. ($>0.7T_g$) and in the SCLR/ high strain rate
- Viscous flow → significant plasticity

  : achieve net-shape forming capability
- Newtonian (high temp. & low stress) vs non-Newtonian (high temp. & applied stress) : associated with the precipitation of nanocrystals

⇩

Homogeneous deformation

8.2.1 Inhomogeneous Deformation

- Low temp. ($<0.5T_g$)/ high stress
- Localized shear band/ 45° to the loading axis
- Strain softening: deformed at lower stress and higher rate

⇩

Catastrophically Failure

Elementary flow events in metallic glasses

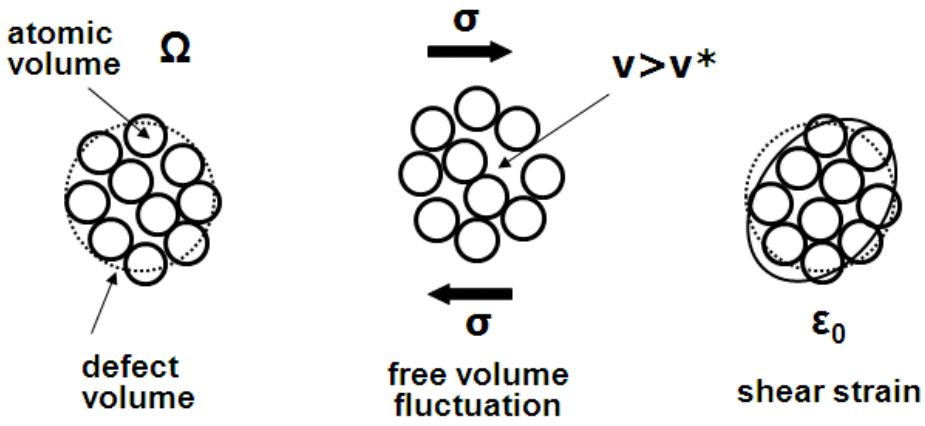

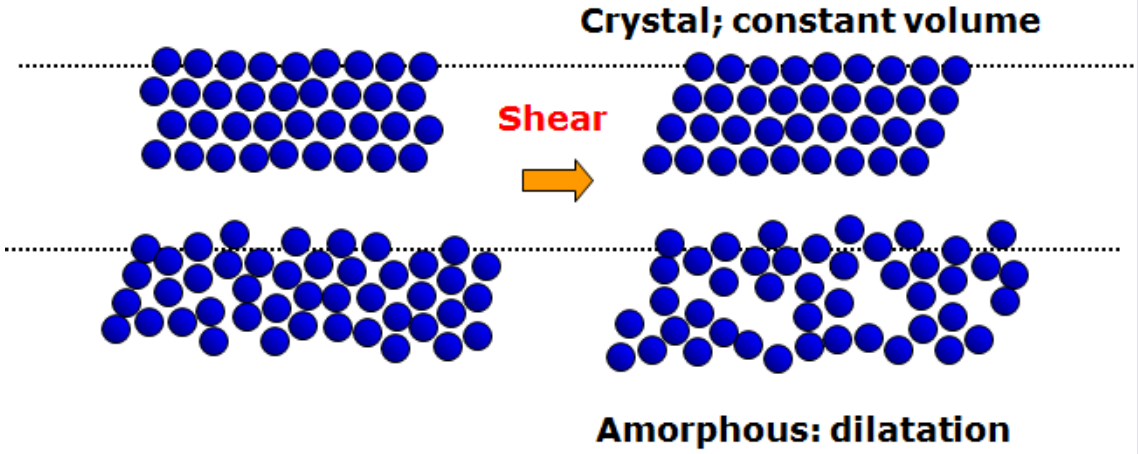

Footprints in sand.
Water quickly disappears underneath

➡ Shear bands form by accumulation of defects during deformation.

nature materials | VOL 5 | JANUARY 2006 | www.nature.com/naturematerials

Effect of local favored structure on SB nucleation

- $Ni_{60}Nb_{40}$: fully amorphous phase

S=0.016 mm/sec

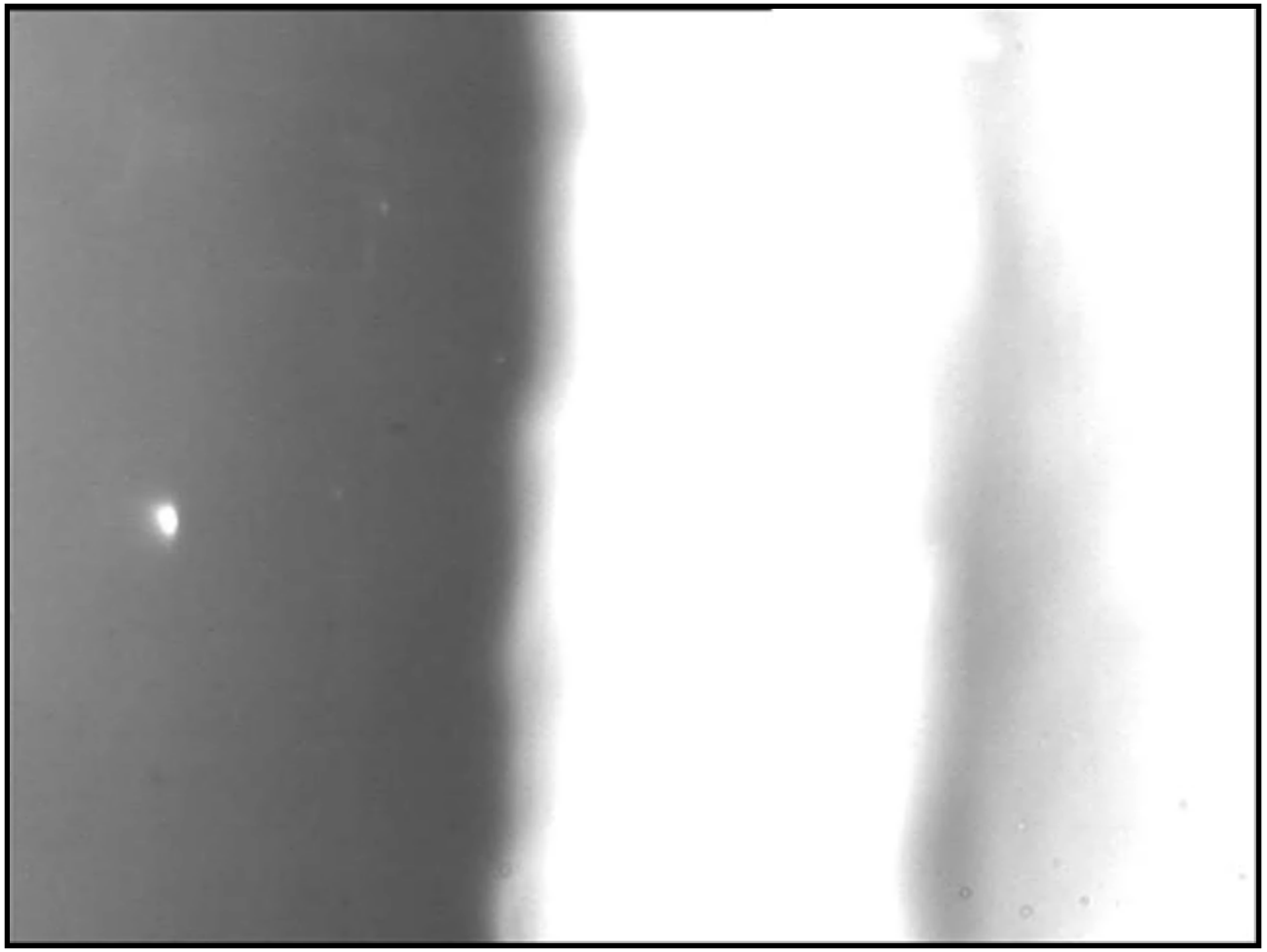

100 μm

Formation of multiple shear bands during deformation

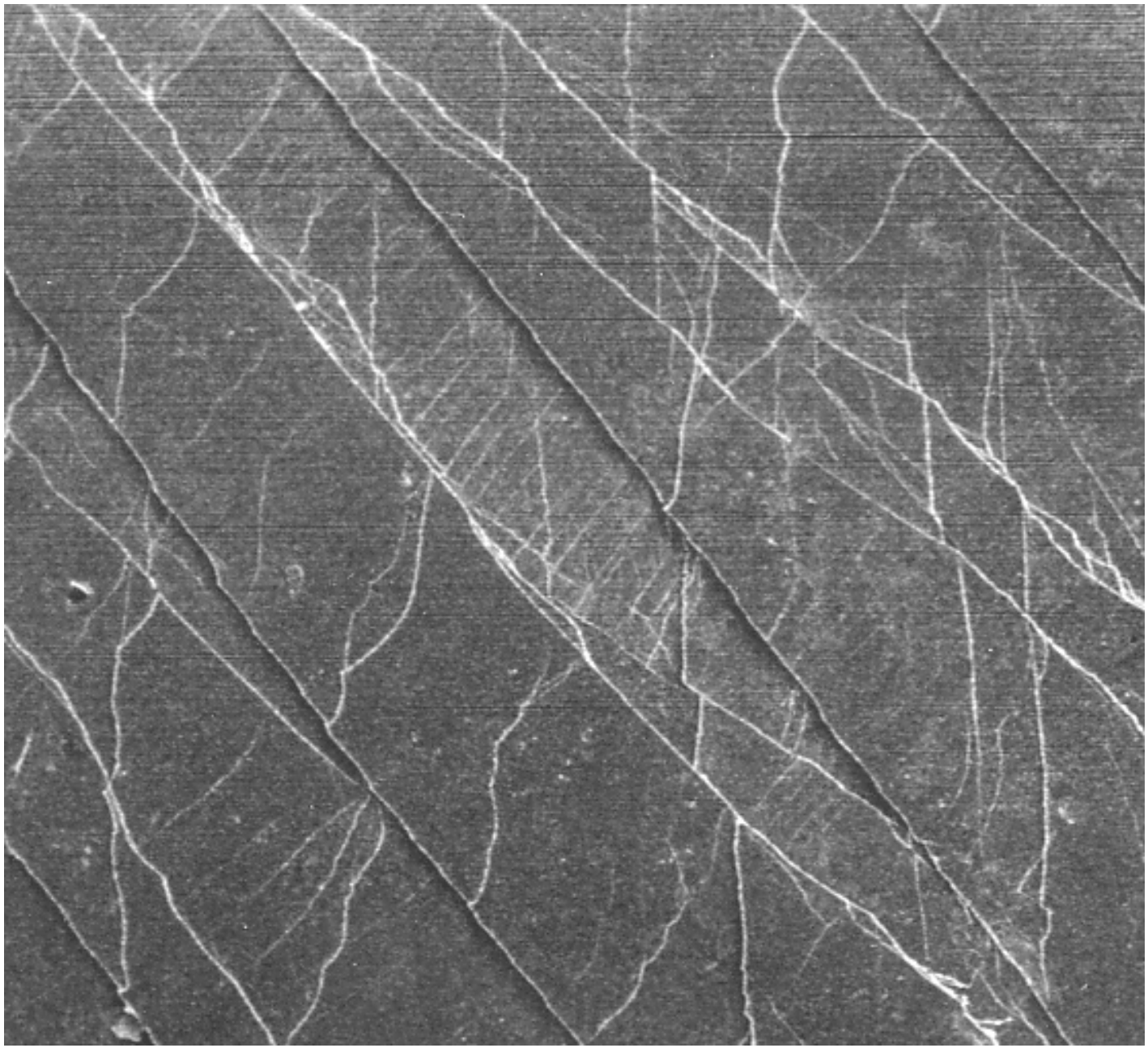

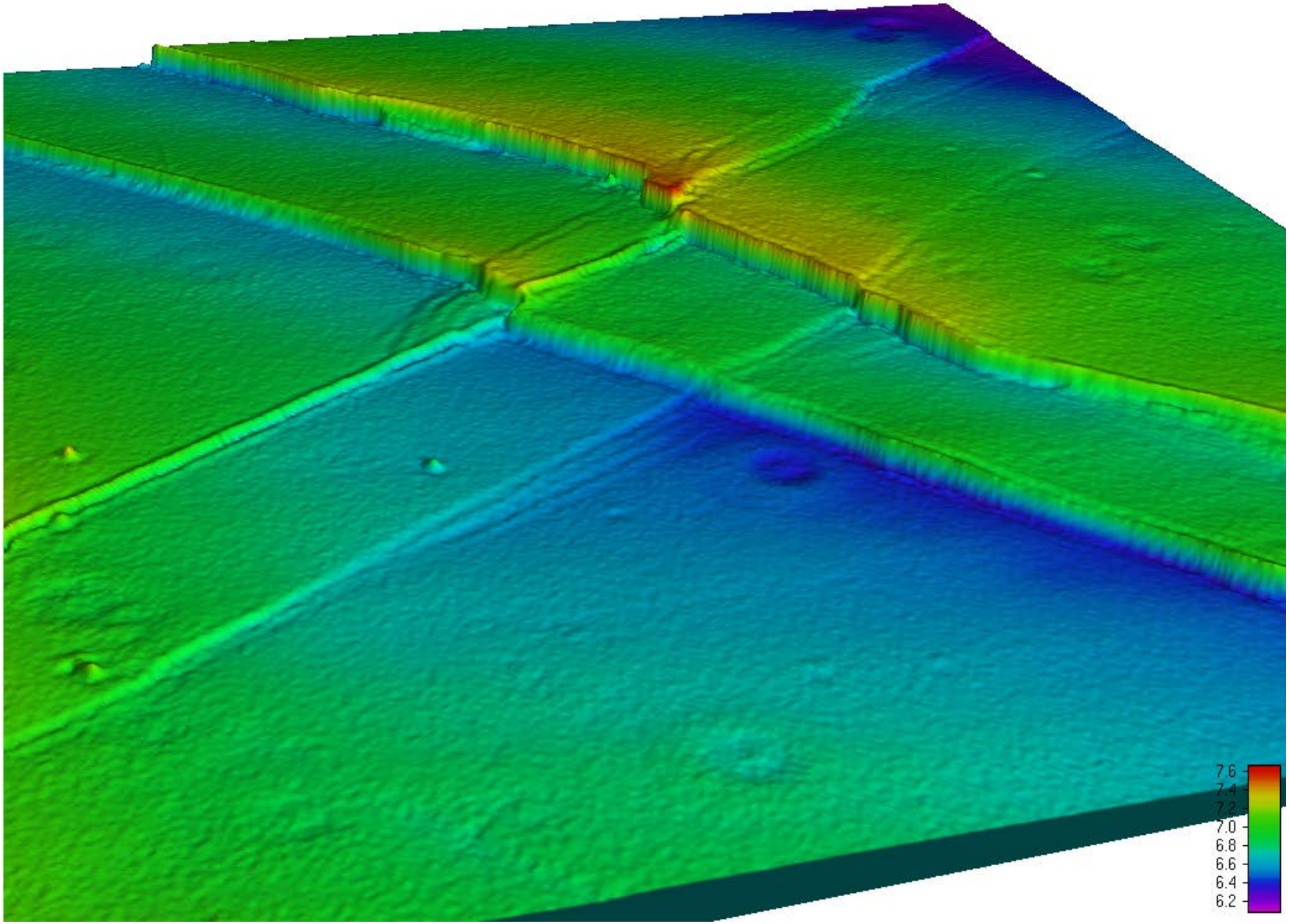
7.6
7.4
7.2
7.0
6.8
6.6
6.4
6.2

Formation of shear bands : variation of free volume

Shear bands form by **accumulation of defects** during deformation.

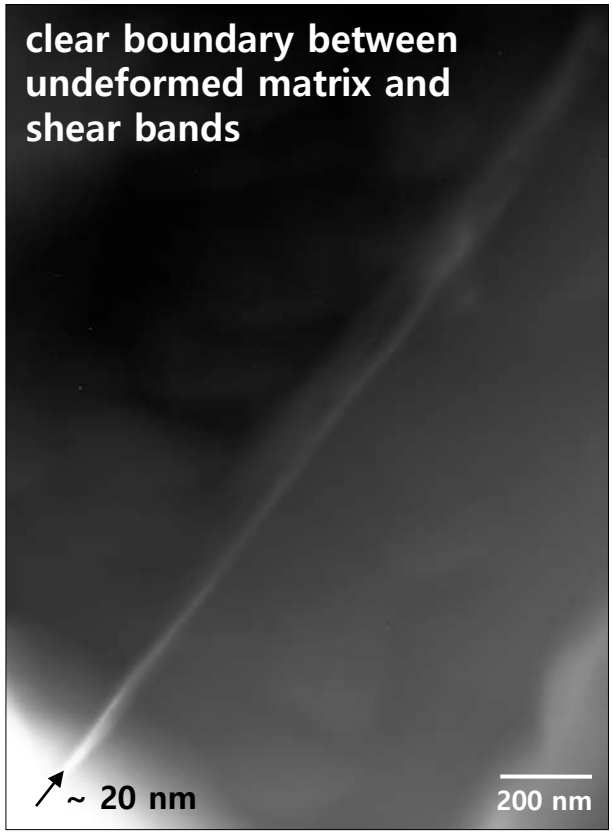

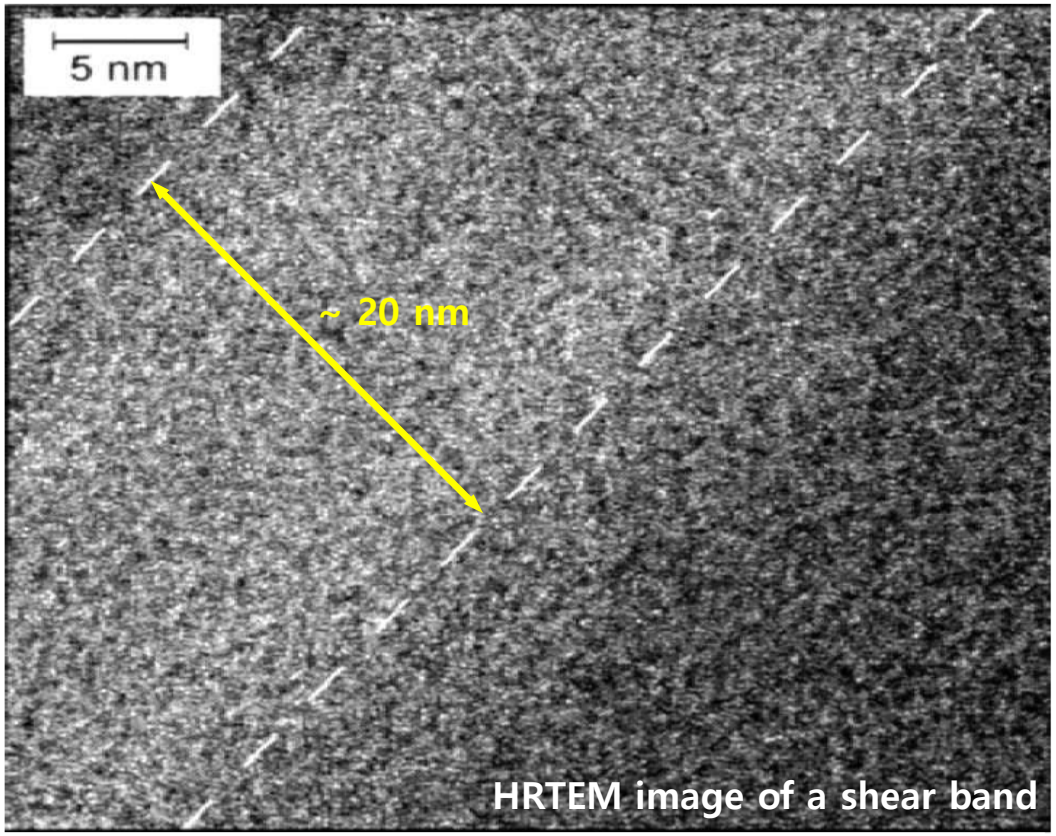

Shear deformed areas with the **same composition** & **different density of free volume**

Shear band nucleation and propagation: strain softening

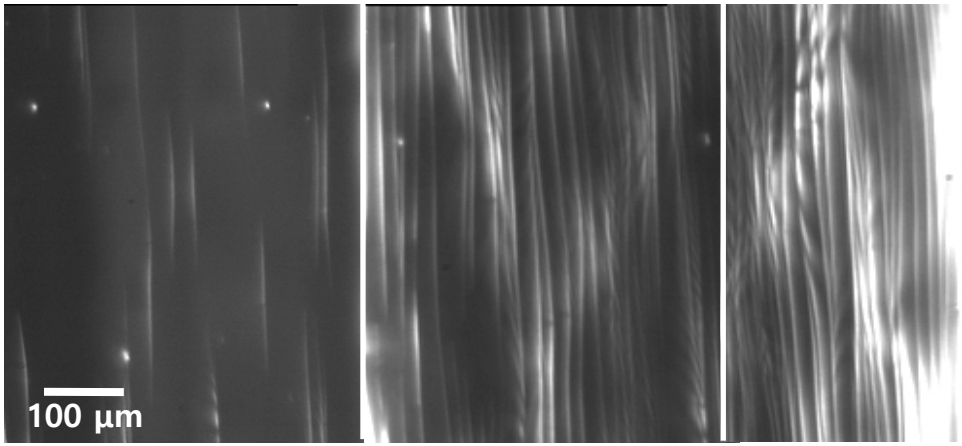

Shear band formation and propagation in the ribbon bending test

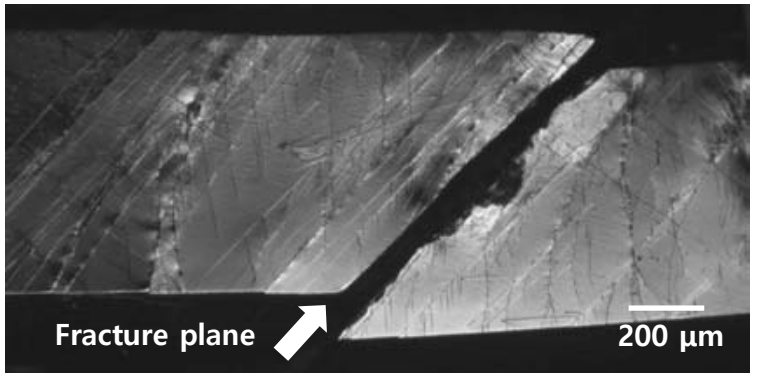

Formation of multiple shear bands in an $Ni_{50}Pd_{30}P_{20}$ BMG specimen subjected to compression testing.
K. Wang et al. / *Acta Mater.* ***56*** *(2008)* 2834.

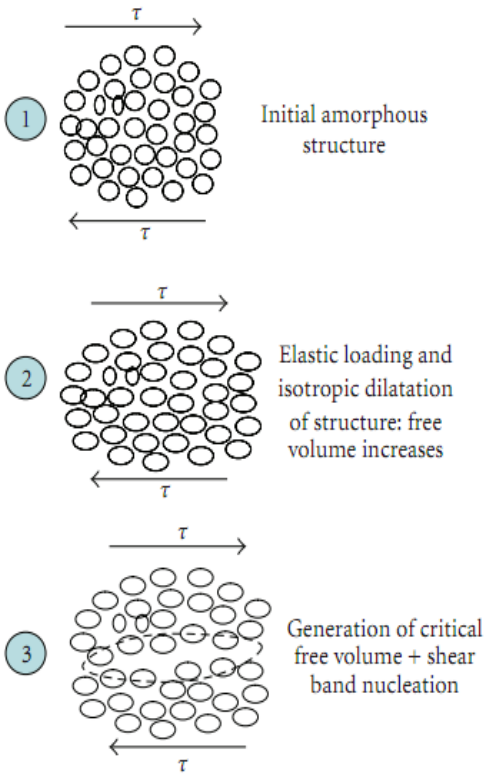

Plastic deformation of metallic glass

controlled by shear band behavior **Nucleation & Propagation**

Excess volume ➡ **Connect to form a shear band**

Plastic strain localized into these shear bands ➡ **Catastrophic failure**

Elastic energy rises local temperature

Decrease in the viscosity ➡ **Shear softening**

Enhancement of ductility ····· **Increase of the shear band density**

SB nucleation and propagation : Multiple serrations, observed only at slow strain rates → temperature rise

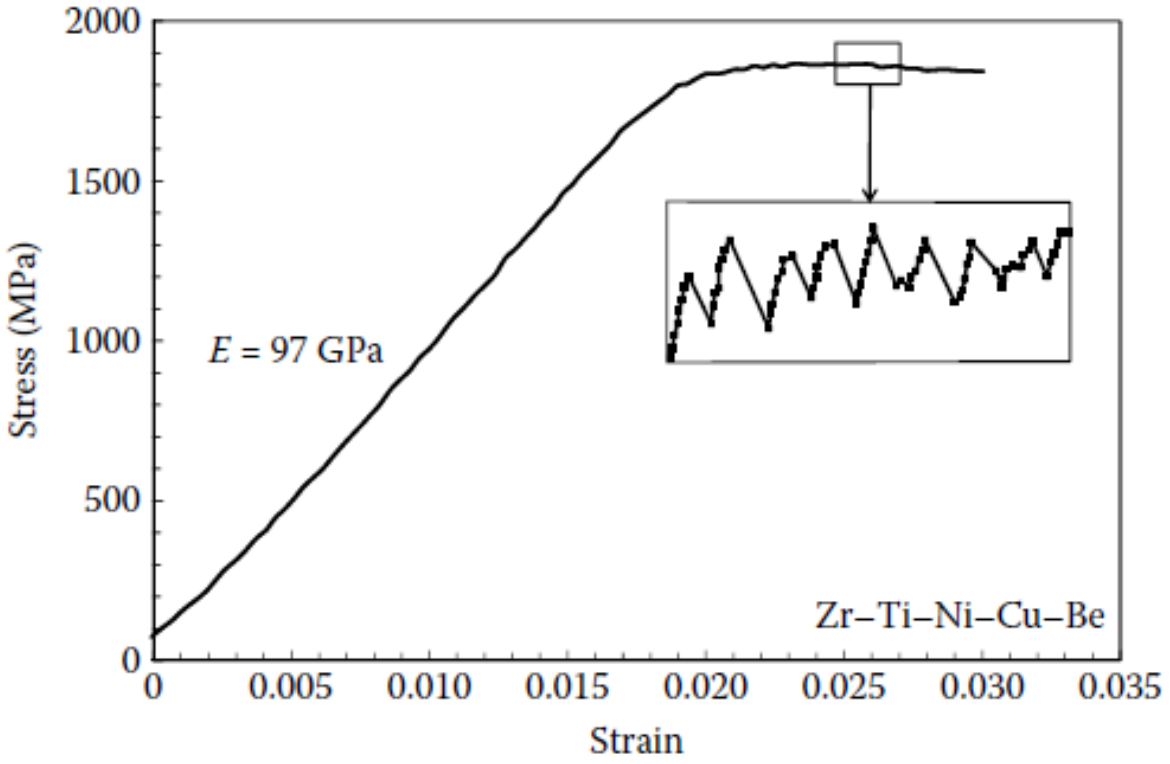

FIGURE 8.1
Compressive stress–strain curve for $Zr_{40}Ti_{14}Ni_{10}Cu_{12}Be_{24}$ BMG alloy tested at a strain rate of $1 \times 10^{-4} s^{-1}$. (Reprinted from Wright, W.J. et al., *Mater. Trans.*, 42, 642, 2001. With permission.)

SB nucleation and propagation : Multiple serrations

→ temperature rise

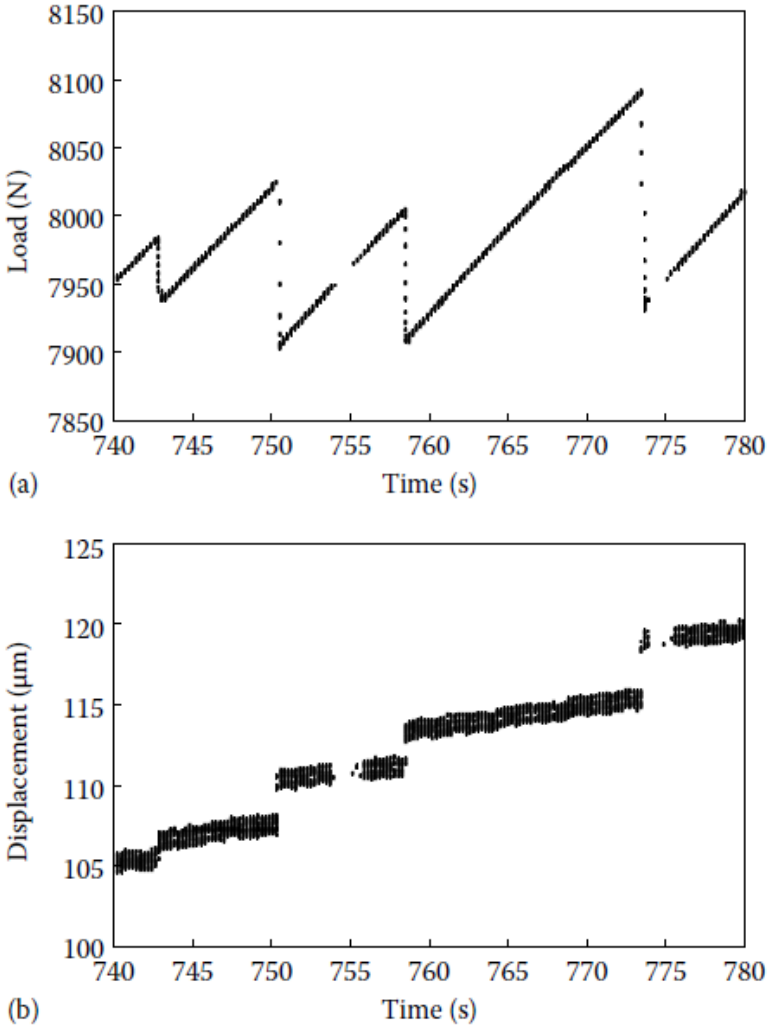

FIGURE 8.2
(a) Load as a function of time and (b) total displacement as a function of time in the serrated flow region of the $Zr_{40}Ti_{14}Ni_{10}Cu_{12}Be_{24}$ BMG alloy tested in uniaxial compression. (Reprinted from Wright, W.J. et al., *Mater. Trans.*, 42, 642, 2001. With permission.)

Serrated flow is also observed during nano-indentation,

but only at "slow loading rates". Activation of each individual shear band is associated with the occurrence of a discrete "pop-in" event (sudden rise in load).

High loading rate → multiple shear bands → smooth load-displacement curve

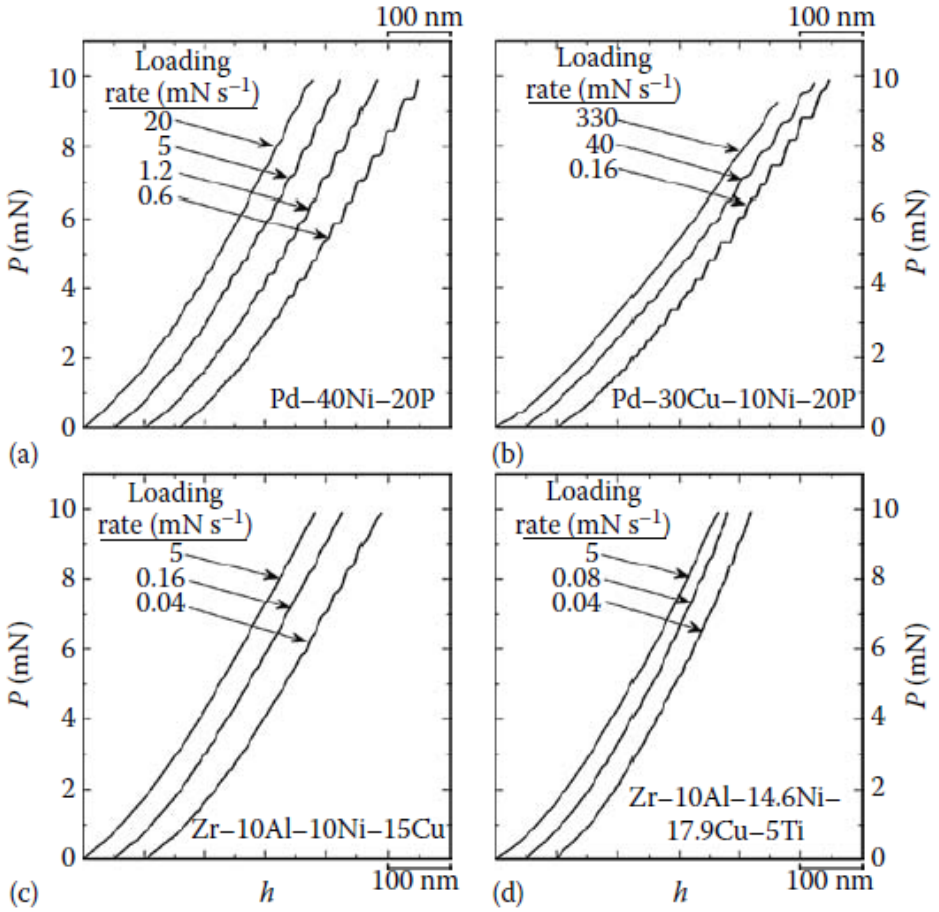

FIGURE 8.3

Typical load–displacement (P–h) curves measured on the loading portion of nanoindentation experiments, for four different BMGs investigated. (a) $Pd_{40}Ni_{40}P_{20}$, (b) $Pd_{40}Cu_{30}Ni_{10}P_{20}$, (c) $Zr_{65}Al_{10}Ni_{10}Cu_{15}$, and (d) $Zr_{52.5}Al_{10}Ni_{14.6}Cu_{17.9}Ti_5$. Curves are offset from the origin for clear viewing, and the rate of indentation loading is specified in each graph. (Reprinted from Schuh, C.A. and Nieh, T.G., *Acta Mater.*, 51, 87, 2003. With permission.)

8.4 Temperature rise at shear bands

Most of the plastic strain is localized in narrow shear bands, which form approximately on the planes of maximum resolved shear stress. The inhomogeneous flow in metallic glasses appears to be related to a local decrease in the viscosity in shear bands. One of the reasons suggested for this was the local adiabatic heating that could lead to a substantial increase in the temperature.

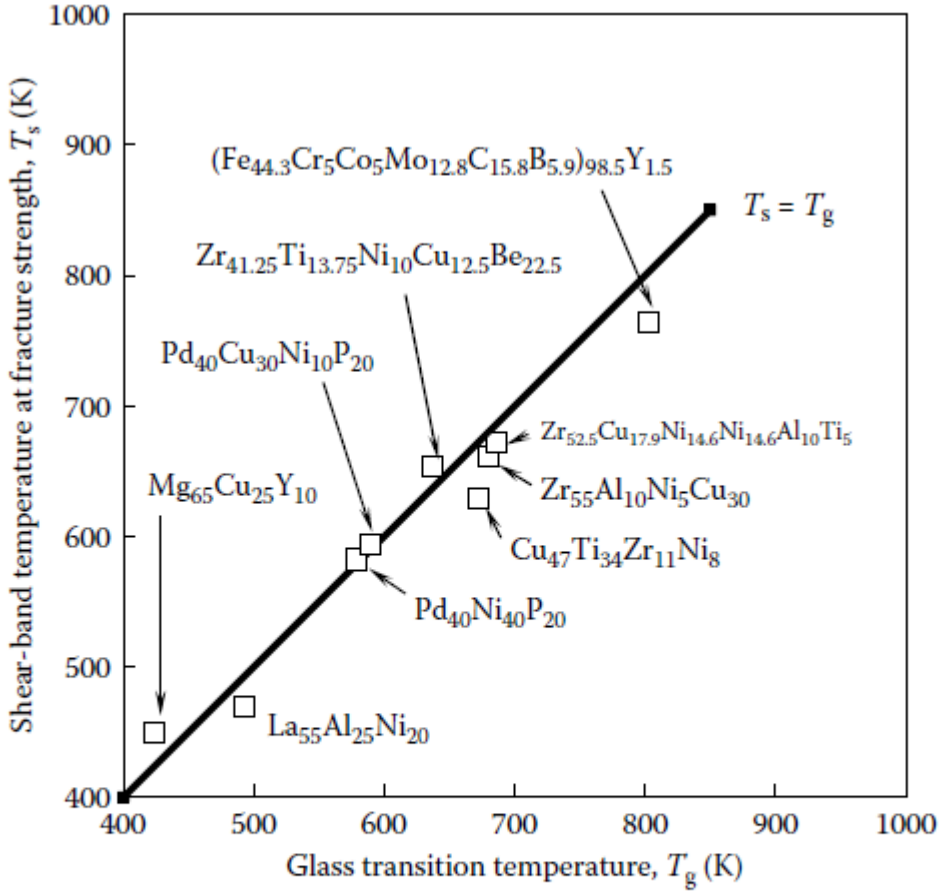

FIGURE 8.8
Temperature rise, ΔT in the shear bands at the time of fracture for different BMG alloys plotted against the glass transition temperature, T_g. (Reprinted from Yang, B. et al., *J. Mater. Res.*, 21, 915, 2006. With permission.)

8.4 Temperature rise at shear bands

Most of the plastic strain is localized in narrow shear bands, which form approximately on the planes of maximum resolved shear stress. The inhomogeneous flow in metallic glasses appears to be related to a local decrease in the viscosity in shear bands. One of the reasons suggested for this was the local adiabatic heating that could lead to a substantial increase in the temperature.

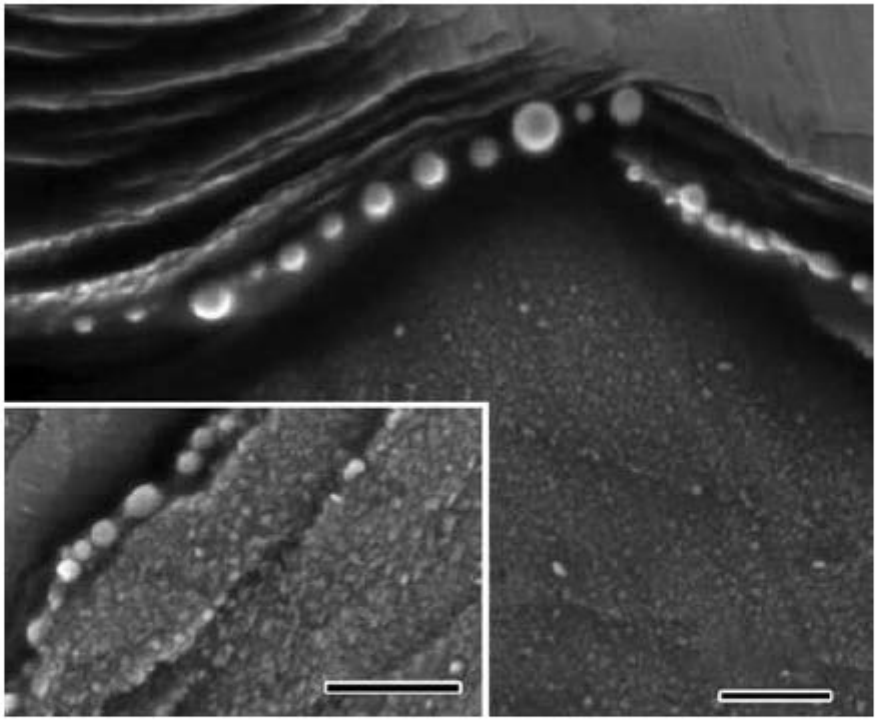

FIGURE 8.9
Scanning electron micrograph of the surface of $Zr_{41.2}Ti_{13.8}Cu_{12.5}Ni_{10}Be_{22.5}$ BMG, which was originally coated with a tin coating. During deformation, the "fusible coating" had melted near the shear bands. The round shape of the tin beads clearly suggests that the coating had melted due to the temperature rise as a result of deformation and had resolidified. The bar in the micrographs corresponds to 1 μm. (Reprinted from Lewandowski, J.J. and Greer, A.L., *Nat. Mater.*, 5, 15, 2006. With permission.)

8.4.1 Nanocrystallization near Shear Bands

TEM analysis after bend test in Al-based ribbon

* **Compressive region of amorphous $Al_{90}Fe_5Gd_5$ (at - 40℃)**

: A high density of nanocrystals is observed within shear bands.

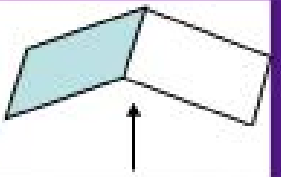

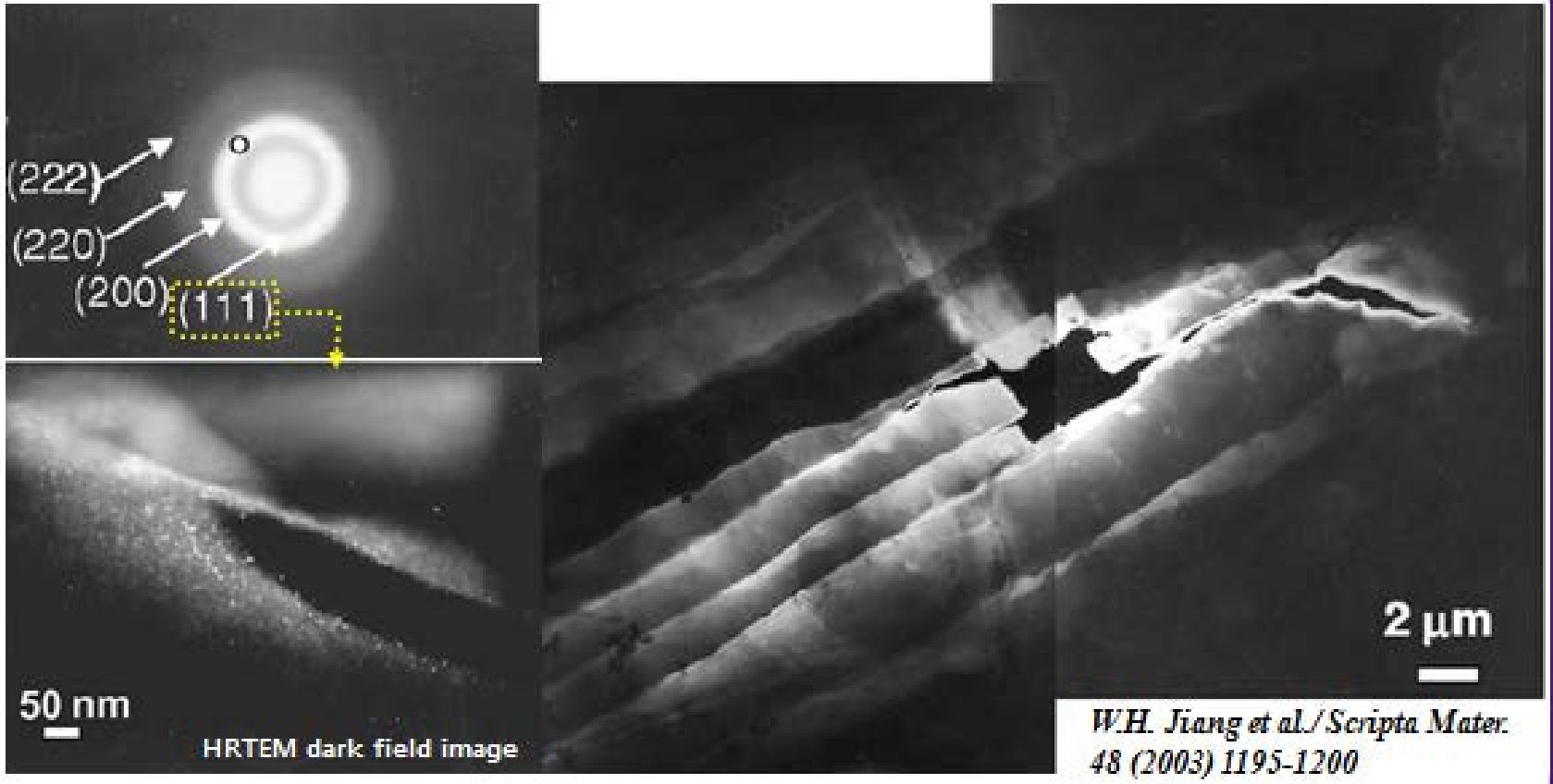

W.H. Jiang et al./ Scripta Mater. 48 (2003) 1195-1200

Low GFA (unstable Amor. Matrix) → **Severe plastic deformation** → **Precipitation of nanocrystals within shear bands**

TEM analysis after severe compressive loading

* Quasi-forming $Ti_{40}Zr_{29}Cu_9Ni_8Be_{14}$ BMG exhibits large plastic strain.

: nanocrystals is observed within shear bands.

H.J. Chang et al./ Scripta Mater. 55 (2006) 509-512

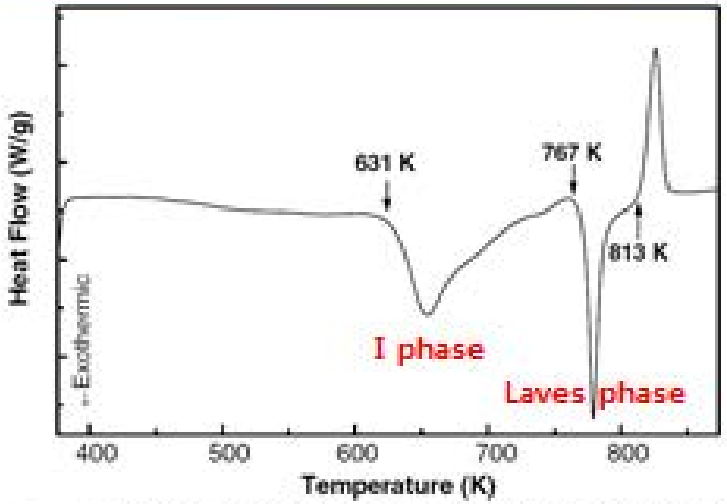

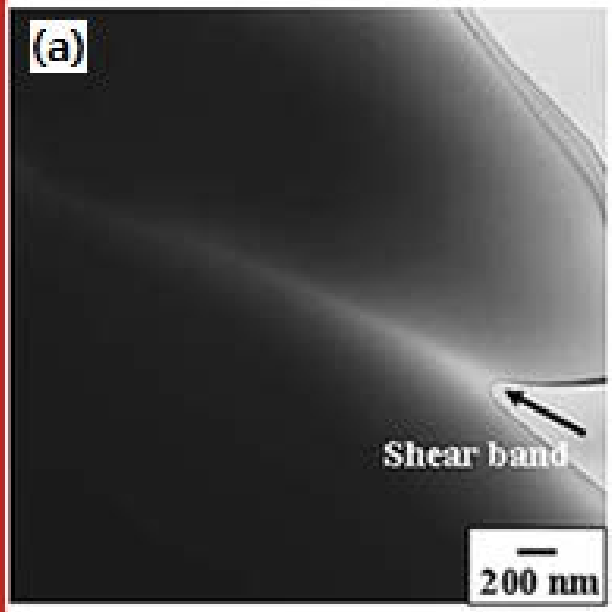

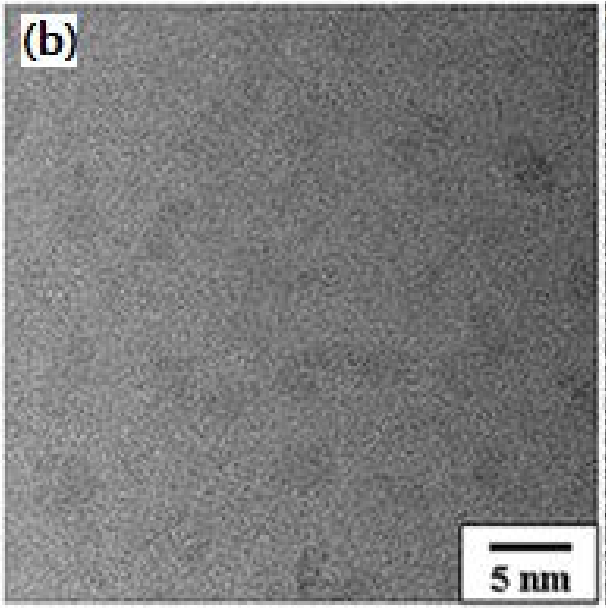

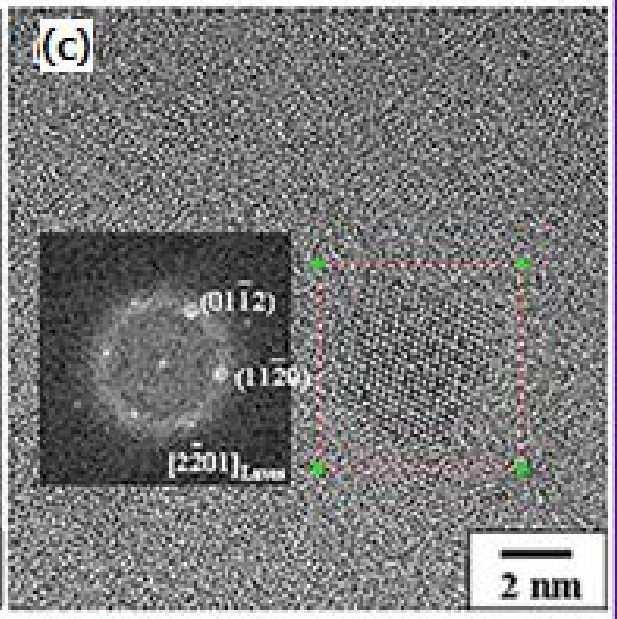

Unstable Amor. Matrix ➡ Severe plastic deformation ➡ Precipitation of nanocrystals within shear bands

TEM analysis after severe compressive loading

* Mg-rich $Mg_{80}Cu_{15}Gd_5$ BMGC ~ large plastic strain

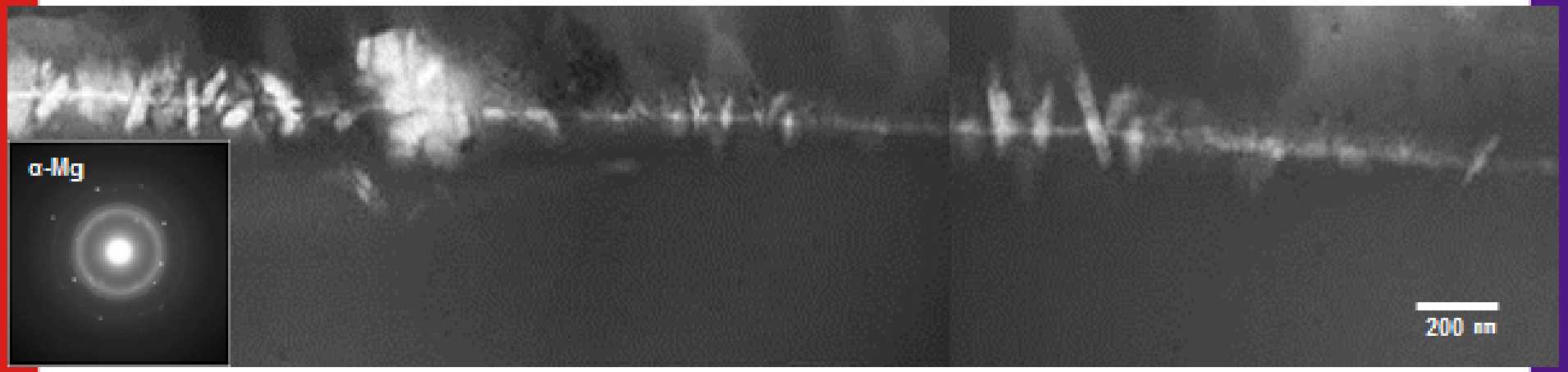

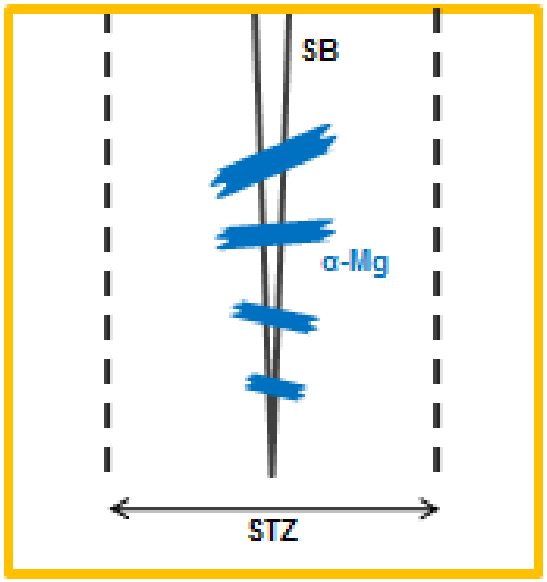

Precipitation of several hundreds nm scale α-Mg in SB & STZ region occurs during the severe compressive deformation, which is related to relatively low T_g (or T_x) value as well as unstable amorphous matrix in Mg-rich BMGC.

J.I. Lee will present the detail at July 8 (11: 45, room E7)

Unstable Amor. Matrix & relatively low T_g (or T_x) ➡ Severe plastic deformation ➡ Precipitation of nanocrystals in SB and STZ region